

inactive per T.T. Hill memo to EBG -  
3/22/55 mtd 3/31/55

9 FEB 1948



# RESEARCH MEMORANDUM

for the

Bureau of Aeronautics, Navy Department

GROUND TESTS OF A RADIAL AIR-COOLED ENGINE TO CORRECT A POOR  
CIRCUMFERENTIAL PRESSURE-RECOVERY DISTRIBUTION

By

James J. Gallagher

Langley Memorial Aeronautical Laboratory  
Langley Field, Va.

~~UNCLASSIFIED~~  
~~PROPRIETARY~~  
~~RESTRICTION~~

## NATIONAL ADVISORY COMMITTEE FOR AERONAUTICS

WASHINGTON

JAN 29 1948

NACA LIBRARY  
LANGLEY MEMORIAL AERONAUTICAL  
LABORATORY  
Langley Field, Va.

inactive



NACA RM No. SL7L10

NATIONAL ADVISORY COMMITTEE FOR AERONAUTICS

RESEARCH MEMORANDUM

for the

Bureau of Aeronautics, Navy Department

GROUND TESTS OF A RADIAL AIR-COOLED ENGINE TO CORRECT A POOR  
CIRCUMFERENTIAL PRESSURE-RECOVERY DISTRIBUTION

By James J. Gallagher

SUMMARY

This report presents the results of the tests of a power-plant installation to improve the circumferential pressure-recovery distribution at the face of the engine. An underslung "C" cowling was tested with two propellers with full cuffs and with a modification to one set of cuffs. Little improvement was obtained because the base sections of the cuffs were stalled. A set of guide vanes boosted the over-all pressures and helped the pressure recoveries for a few of the cylinders. Making the underslung cowling into a symmetrical "C" cowling evened the pressure distribution; however, no increases in front pressures were obtained. The pressures at the top cylinders remained low and the high pressures at the bottom cylinders were reduced. At higher powers and engine speeds, the symmetrical cowling appeared best from the standpoint of over-all cooling characteristics.

INTRODUCTION

An investigation of the aerodynamic characteristics of several cowling configurations of the XSC-1 has been conducted at the Langley 16-foot high-speed-tunnel ground test stand. Two different cowlings, several propeller-cowling combinations, and a set of guide vanes were tested in an attempt to improve the total pressure-recovery distribution at the face of the engine.

The original model was a revision of the power-plant installation which had been tested previously in the Langley 16-foot high-speed tunnel. The tunnel tests showed a very large variation in circumferential pressure distribution at the face of the engine for low speeds especially for the climb condition. Total pressure recoveries at the top of the engine were in some cases one-half to one-third of the total pressure recoveries at the bottom of the engine (reference 1). These

low pressures, however, provided the necessary mass flow of cooling air with cowling flaps full open to cool the cylinders properly. The situation, nevertheless, might arise in similar installations where the low top recoveries may cause the cooling of these cylinders to be marginal. Excessive pressures at the face of the lower cylinders provided an excess of cooling air which increased the cooling drag and overcooled the cylinders. This report presents the results of the investigation made to remedy these conditions.

#### DESCRIPTION OF MODEL

The original model used was a modification of the XSC-1 power-plant installation which was used in the wind-tunnel tests of reference 1. The turbosupercharger, intercoolers, and intercylinder ducts were removed and a new exhaust system and tail pipe were fabricated. The model is shown mounted on the ground test stand in figure 1. The cowling is an underslung variation of an NACA "C" cowling. The two ducts in the underslung lip supply air to the oil coolers.

The engine is a Wright R1820-56, nine-cylinder, forged-head radial engine rated at 1300 brake horsepower at 2600 rpm. The conventional nose was replaced with a 3:2 gear-reduction torque nose for measuring engine power. The standard baffles used closed the spaces between the cylinders and extended forward to the center line of the cylinders.

The underslung cowling was tested with three propeller-cuff combinations. A 10-foot four-blade Hamilton Standard hydromatic propeller (blade number A6529-A-14), with full cuffs, the same as was used in the tunnel tests, is shown in figure 2. These cuffs were then modified by decreasing the twist angle  $10^\circ$  at the base of the cuff and increasing the width of the cuff. A sketch of the modification is shown in figure 3 and the modified cuffs installed on the propeller are shown in figure 4. A 10-foot four-blade Curtiss electric propeller from a production SC-1 airplane is shown in figure 5. The propeller blades were Curtiss 528-1C2-12 with full cuffs.

A set of eight guide vanes (fig. 6) was then installed. The vanes were purposely made thick to cut down the inlet expansion ratio and to cover up a large percentage of the intercylinder space. The vanes extended to the cowling lip. The nose of the vane was a circular arc, the bisector of which made an angle of  $30^\circ$  with the axis of propeller rotation.

The cowling was modified to a symmetrical "C" cowling by installing a new bottom half identical with the top half. (See fig. 2.) A sketch of both cowlings is shown in figure 7 and coordinates of each are given in table I. The oil cooler and oil-cooler ducts were removed and for purposes of the ground tests located in the propeller slipstream.

## APPARATUS

In addition to the usual complement of engine instruments, provisions were made for measuring fuel flow, weight flow of charge air, cylinder temperatures, and air-pressure drop across the cylinders.

Fuel flow was measured by means of a rotameter and also a weigh tank. The weight of charge air was measured by a calibrated venturi mounted on the top of the model as shown in figure 1. All temperatures were measured on a self-balancing recording potentiometer. Spark-plug-gasket thermocouples were used to indicate cylinder-head temperature. Cylinder-cooling pressures were measured by means of total-pressure and static-pressure tubes installed on each cylinder (fig. 8). The total-pressure tubes on the right and left sides of the heads were installed  $3/8$  of an inch inside of the baffles. The top of the head total-pressure tube was similarly installed in its baffle and the rear of the head static tube was installed in the curl of the baffle on the left side of the cylinder.

## SYMBOLS

bhp	brake horsepower
$C_p$	power coefficient $\left( \frac{P}{\rho n^3 D^5} \right)$
D	propeller diameter, feet
h	total pressure at face of engine, inches of water
n	propeller revolutions per second
P	engine power, foot-pounds per second
p	static pressure at rear of head, inches of water
$\Delta p$	engine cooling pressure drop, inches of water
rpm	engine revolutions per minute
q	dynamic pressure, pounds per square foot $\left( \frac{1}{2} \rho v^2 \right)$
$t_a$	free-stream stagnation air temperature, $^{\circ}F$
$t_h$	spark-plug-gasket temperature, $^{\circ}F$

$t_e$	average spark-plug-gasket temperature, °F
$t_g$	mean effective gas temperature, °F
$V$	stream velocity, feet per second
$W_e$	charge air to engine, pounds per second
$\rho$	air density, slugs per cubic foot
$\rho_s$	standard air density, 0.002378 slug per cubic foot
$\sigma$	density ratio $\left( \frac{\rho}{\rho_s} \right)$

#### TEST METHOD

All the configurations were tested at the same conditions. A series of runs was made at engine speeds varying from 1630 rpm to 2400 rpm at a constant power coefficient  $C_p$  of 0.125. Another series was run at a constant engine speed of 1800 rpm with the power coefficient varying from 0.08 to 0.16.

Test runs were made only when interference from wind was at a minimum. All the cylinder front and rear pressures, cylinder-head temperatures, engine fuel-air ratio, atmospheric temperature, and barometric pressure were measured. For all runs the carburetor mixture control was set at automatic rich.

#### DISCUSSION

Figure 9 shows the pressure distribution at the face of the engine for the climb condition as obtained in the wind-tunnel tests. This distribution is very similar to the ones obtained in the ground tests (fig. 10) and justifies the use of the ground tests for this exploratory investigation. Figure 10 presents the temperature and pressure distributions around the engine for the original underslung cowling with the normal Hamilton Standard propeller cuffs. The engine speed and power were varied, but  $C_p$  was held constant. Variations in both the pressure and temperature distributions around the engine increased with increasing engine speed. Figure 11 is for the same configuration but with the engine speed held constant and  $C_p$  varied by changing the power.

There was little change in the pressure recoveries at the face of the engine; the bottom of the engine showed some slight gain. The temperature pattern shows the same trend throughout the range of values of  $C_p$  run, the temperatures increasing with increasing power.

It can be shown that when  $C_p$  is held constant and the engine rpm is varied, the blade angle remains essentially constant. Therefore the poor pressure and temperature distribution was due chiefly to blade and cuff sections. With increasing rpm the base sections of the cuff became stalled and produced little or no increase in lift, but considerable rotation, while the sections farther out radially produced higher pressure rises. In the case where the rpm was held constant and  $C_p$  varied, it appears that the cuff sections were stalled or were working near the region of maximum lift coefficient because increases in blade angle effected by changing  $C_p$  made relatively small change in the front pressures.

It is believed that the cause of the asymmetrical total pressure recoveries is the relative effectiveness of the propeller and cuff sections which influence the pressures in front of the top and bottom cylinders. The underslung lip acts like a duct in conveying pressures to the lower cylinders. The bottom pressures are thus affected by sections which are radially farther out on the blade, are at less angle of attack, and are thinner than the cuff sections which affect the top pressures. The bottom pressures therefore would be expected to be higher than those for the top cylinders.

The modification made to the Hamilton Standard propeller cuffs was such that the base angle of the cuff was reduced  $10^\circ$ , the thickness ratio of the section was reduced from 46 percent to 40 percent, and the cuff width increased from 10.8 inches to 13.1 inches. Curves for this configuration at a constant  $C_p$  are presented in figure 12. Only a very slight increase in over-all pressure recovery was noted, the average increase being less than  $1/2$  inch of water, but the cylinder-head temperatures were decreased about  $25^\circ$ . These increases in pressure and reductions in temperature are undoubtedly due to the modification to the cuffs. The pressure and temperature patterns for the underslung cowling with the Curtiss electric propeller (fig. 13) are very similar to those with the unmodified Hamilton Standard propeller and show no improvement.

Since the cuff sections at the base of the blades appeared to be stalled, a preliminary investigation was made to find out how much rotation was being imparted to the air. Figure 14 shows the general flow direction by means of tufts installed in the entrance and a deposit of aluminum powder on the push rod covers. Figure 14(a) shows the general flow direction of the air at the entrance of the underslung cowling at an engine speed of 1630 rpm and a  $C_p$  of 0.125 with the

cowling flap full open. Figures 14(b) and 14(c) show the flow direction indicated by aluminum powder deposits for the engine with the symmetrical "C" cowling. Both tufts and powder deposits indicate an air-flow angle of approximately  $45^\circ$  to the face of the engine. This high angularity would be expected to cause the low recoveries for cylinders 2 and 3 since they would be operating in the wake of the propeller governor.

It was believed that compartmenting the air by a set of guide vanes (fig. 6) would reduce the rotational velocity component. The vanes also, by filling the space between the cylinders, cut down the expansion ratio of the cowling inlet and acted like diffusers.

The temperature and pressure patterns for the underslung cowling, modified Hamilton Standard propeller, and guide vanes are shown in figure 15. The individual cylinder front pressures were almost all increased by about 1 inch of water and the distribution made more uniform, cylinders 4, 5, 6, and 7 having nearly the same pressure recoveries. The pattern trends shown in figure 16 are similar to those obtained with the original cowling. Increasing  $C_p$  had only a moderate effect on increasing the front pressures.

The underslung lip was removed and the symmetrical bottom half of the cowling was installed. Temperature and pressure plots are shown in figures 17 and 18. The pressure recoveries are less with the symmetrical cowling than those obtained with the underslung cowling for comparable engine-operating conditions. The circumferential pressure-recovery distribution with the symmetrical "C" cowling, however, is very uniform, the bottom pressures being reduced to approximately the same value as the top pressures. It can be concluded, therefore, that the maldistribution of pressure was due to the underslung lip on the cowling. The constant-engine-speed, variable- $C_p$  runs show the same tendency as all the other configurations.

The previously presented curves show the effect on the pressure distributions of the various configurations; however, the general cooling characteristics are not obvious. In order to evaluate the merits of each configuration, the NACA cooling-correlation method was employed (references 2 to 4). A general statement of the correlation principle is that the ratio of cooling-temperature differential to heating-temperature differential is a function of a relation between internal flow of heating fluid and external flow of cooling fluid. This is expressed symbolically as follows

$$\frac{t_e - t_a}{t_g - t_e} = (\text{constant}) \frac{(W_e)^y}{(\sigma \Delta p)^z}$$

The equation determined in the wind-tunnel tests of the XSC-1 power-plant installation was

$$\frac{t_e - t_a}{t_g - t_e} = 0.532 \frac{W_e^{0.628}}{(\sigma \Delta p)^{0.314}}$$

which can be transformed to

$$\frac{t_e - t_a}{t_g - t_e} = 0.532 \left( \frac{W_e^2}{\sigma \Delta p} \right)^{0.314}$$

An attempt was made to run a complete correlation with the model mounted on the ground stand. Due to the limited range of pressure drops available and the inability to make runs of varying power at a constant value of engine pressure drop, the values of the exponents  $x$  and  $y$  could not be obtained. The engine pressure drop  $\Delta p$  was obtained by averaging all of the front pressures and subtracting the average of all the rear pressures.

The engine was the same as the one used in the tunnel tests so the ground-test data were reduced assuming the exponents and mean effective gas temperature curve obtained previously (reference 5). The assumption is justified since the data correlate very well as shown in figures 19, 20, and 21. The instrumentation was the same, but the baffles were different.

Figure 19 shows little effect on the cooling characteristics of the whole engine of the various propeller and propeller-cuff combinations, the modified cuffs giving a slightly lower curve. Figure 20 compares the vaned and unvaned entrances. The vanes show no noticeable decrease

in  $\frac{t_e - t_a}{t_g - t_e}$  for a given  $\frac{W_e^2}{\sigma \Delta p}$ ; however, the slope of the curve is less.

The decrease in slope is due to the vanes making the pressure recoveries around the entrance more nearly equal. This indicates that at higher powers and low pressure drops the vanes would be more effective in cooling the engine.

The installation of the "C" cowling, by evening out the pressure distribution, also decreased the slope of the correlation curve (fig.21) and was more effective than the vanes. The data all correlated well even though the pressure distributions around the engine for the various configurations were widely different.

## CONCLUSIONS

1. By decreasing the twist angle of the base sections of the propeller cuffs  $10^\circ$  and simultaneously increasing the blade-cuff widths, the front pressure recoveries were increased by about 1/2 inch of water.

2. Installing vanes in the cowling entrance gave slight increases of about 1 inch of water in the front pressure recoveries and tended to make the circumferential pressure distribution more even.

3. The symmetrical "C" cowling provided an even circumferential pressure-recovery distribution, but a slight decrease in over-all pressure recovery was obtained when compared with the other configurations. At higher powers the general cooling characteristics, however, were better with the symmetrical cowling than with the under-slung cowling.

4. In all cases the cowlings appeared to be working behind cuff sections which were stalled or were operating in the neighborhood of maximum lift.

5. The NACA cooling-correlation method provided a good means of evaluating the merits of the configurations and also proved to be useful even when large variations in front pressure distributions were obtained.

Langley Memorial Aeronautical Laboratory  
National Advisory Committee for Aeronautics  
Langley Field, Va.

  
James J. Gallagher  
Aeronautical Engineer

Approved:

  
John V. Becker

Chief of Compressibility Research Division

bbs

## REFERENCES

1. McLellan, Charles H., Runckel, Jack F., and Gallagher, James J.: Tests of the XSC-1 Power-Plant Installation in the LMAL 16-Foot High-Speed Tunnel. I - Aerodynamics. NACA MR No. L4J12, Bur. Aero., 1944.
2. Pinkel, Benjamin, and Ellerbrock, Herman H., Jr.: Correlation of Cooling Data from an Air-Cooled Cylinder and Several Multi-cylinder Engines. NACA Rep. No. 683, 1940.
3. Schey, Oscar W., Pinkel, Benjamin, and Ellerbrock, Herman H., Jr.: Correction of Temperatures of Air-Cooled Engine Cylinders for Variation in Engine and Cooling Conditions. NACA Rep. No. 645, 1938.
4. Pinkel, Benjamin: Heat-Transfer Processes in Air-Cooled Engine Cylinders. NACA Rep. No. 612, 1938.
5. McLellan, Charles H., Runckel, Jack F., and Gallagher, James J.: Tests of the XSC-1 Power-Plant Installation in the LMAL 16-Foot High-Speed Tunnel. II - Cooling. NACA MR No. L4J12a, Bur. Aero., 1944.

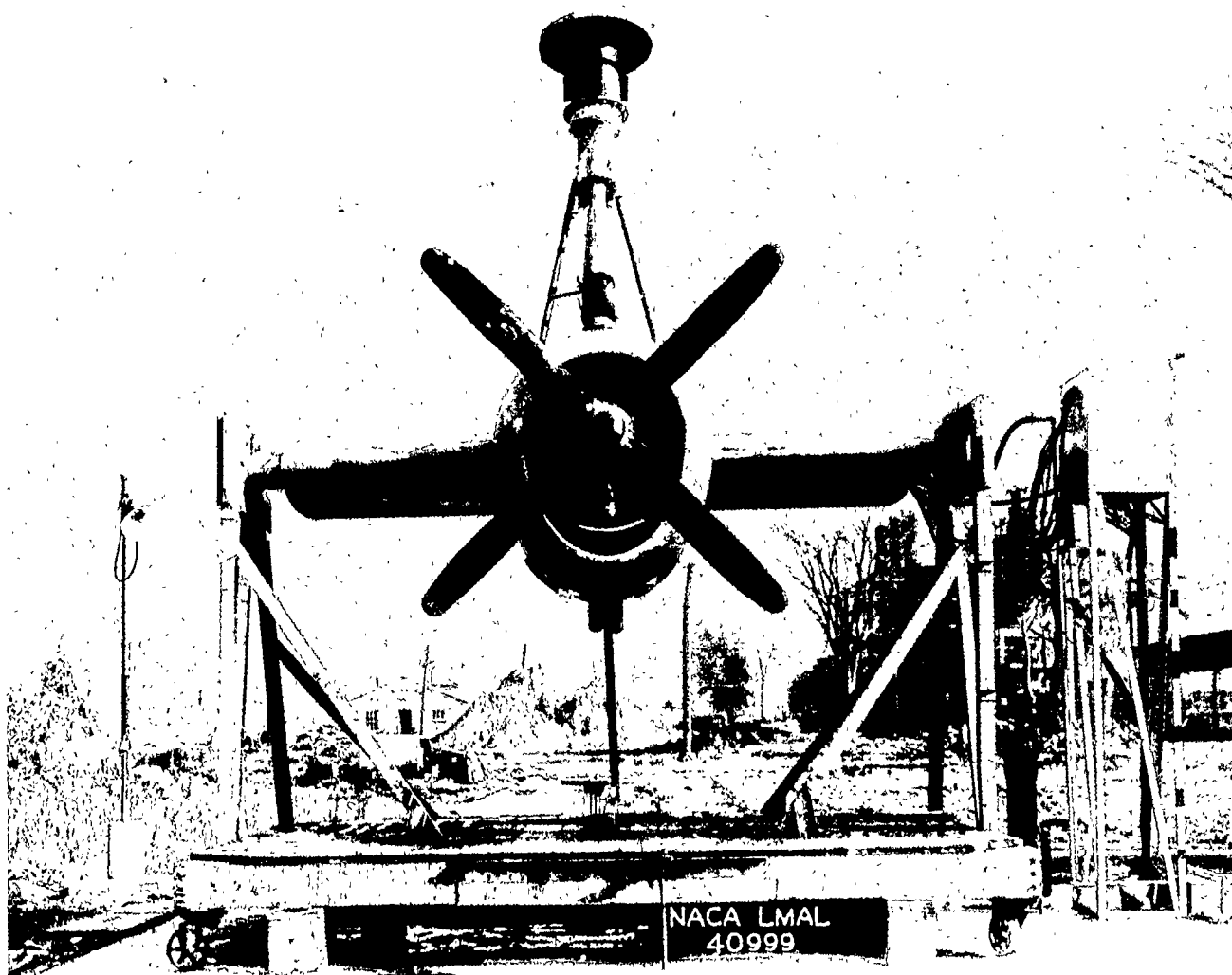
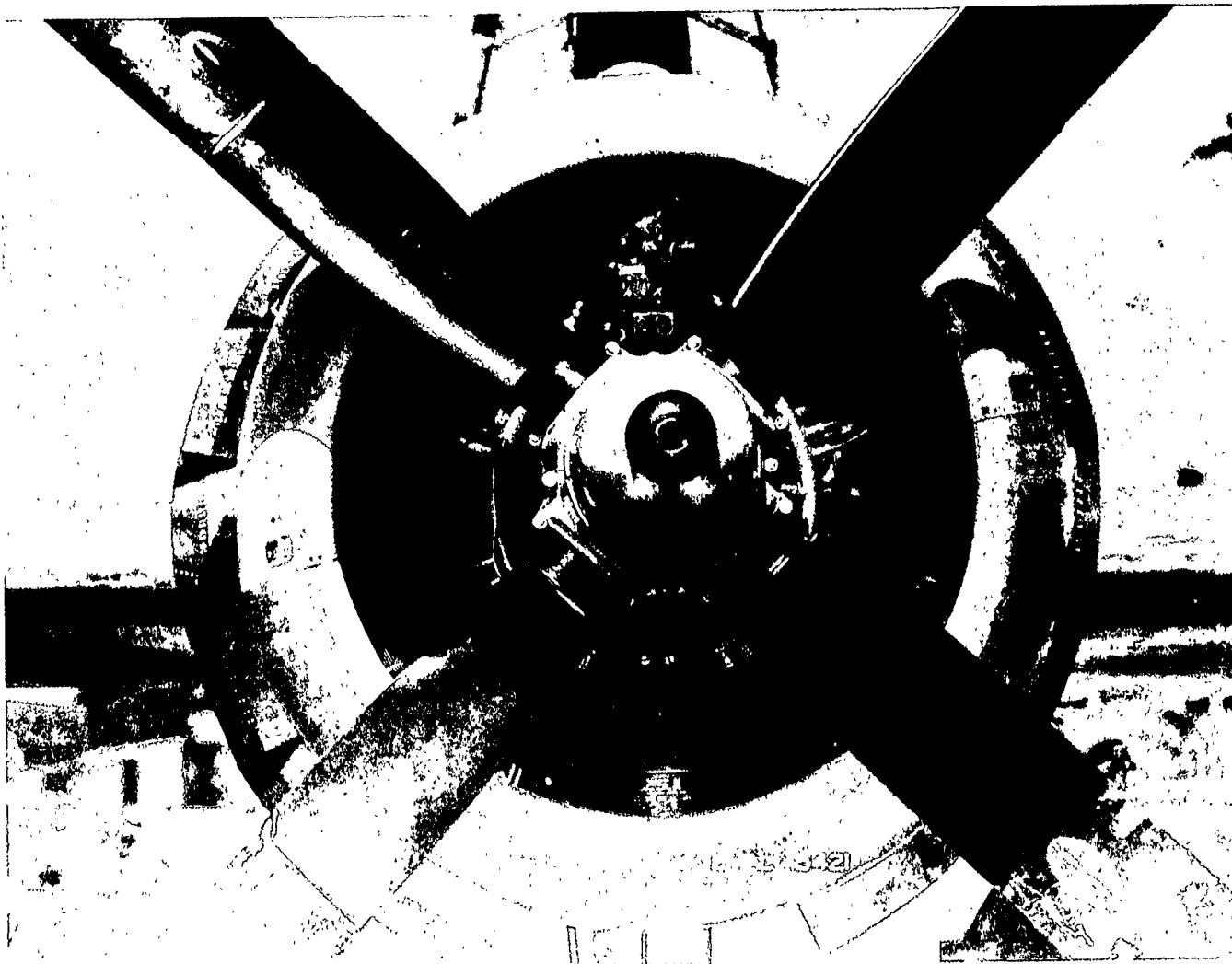


Figure 1.- General view of model mounted on the ground test stand showing the underslung cowling and the charge-air induction system.



NACA FM No. 517110

Figure 2.- Front view of full cuffs on Hamilton Standard hydromatic propeller, symmetrical cowling.

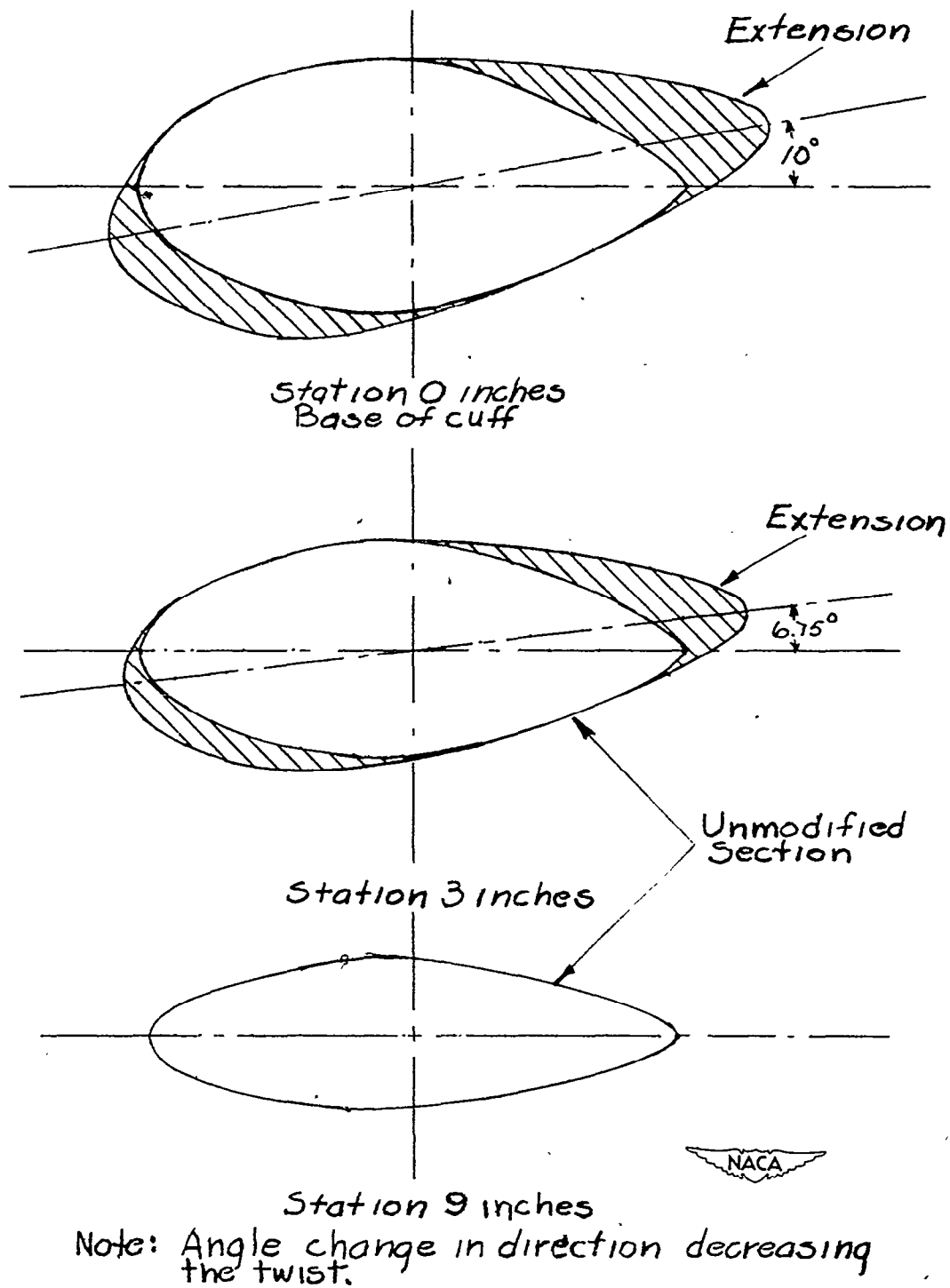
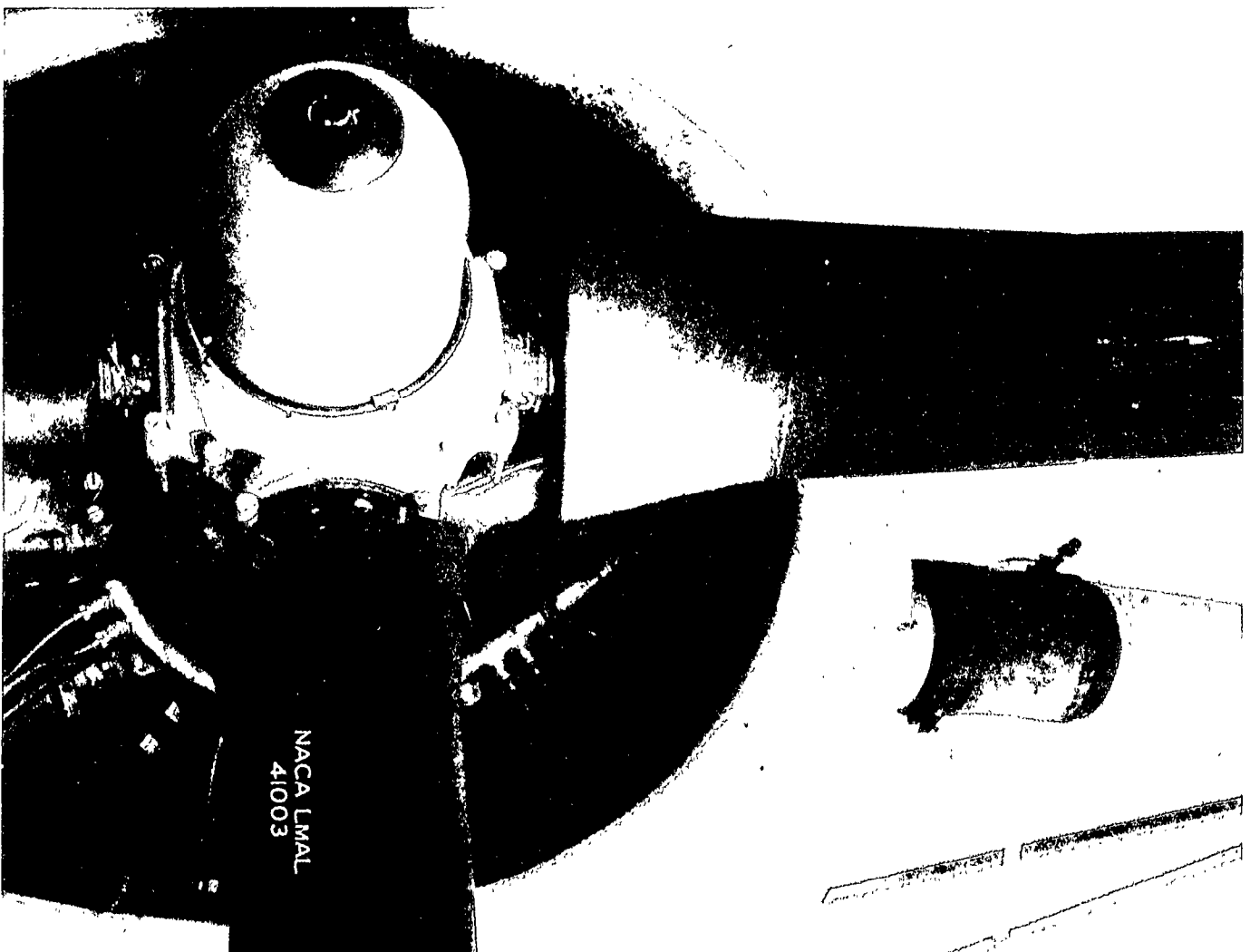
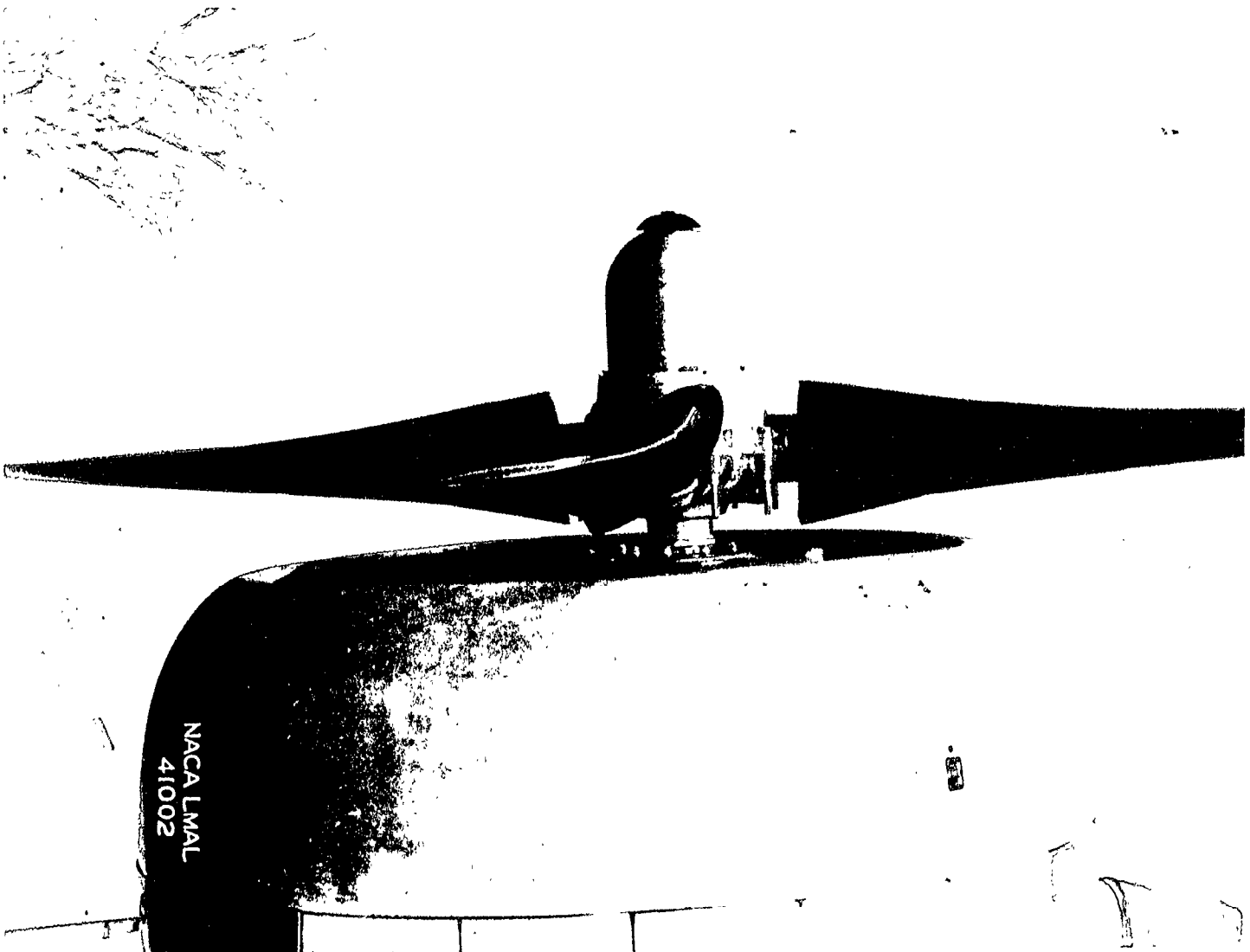


Figure 3.- Sketch of modification to Hamilton Standard propeller cuffs.



(a) Front quarter view.

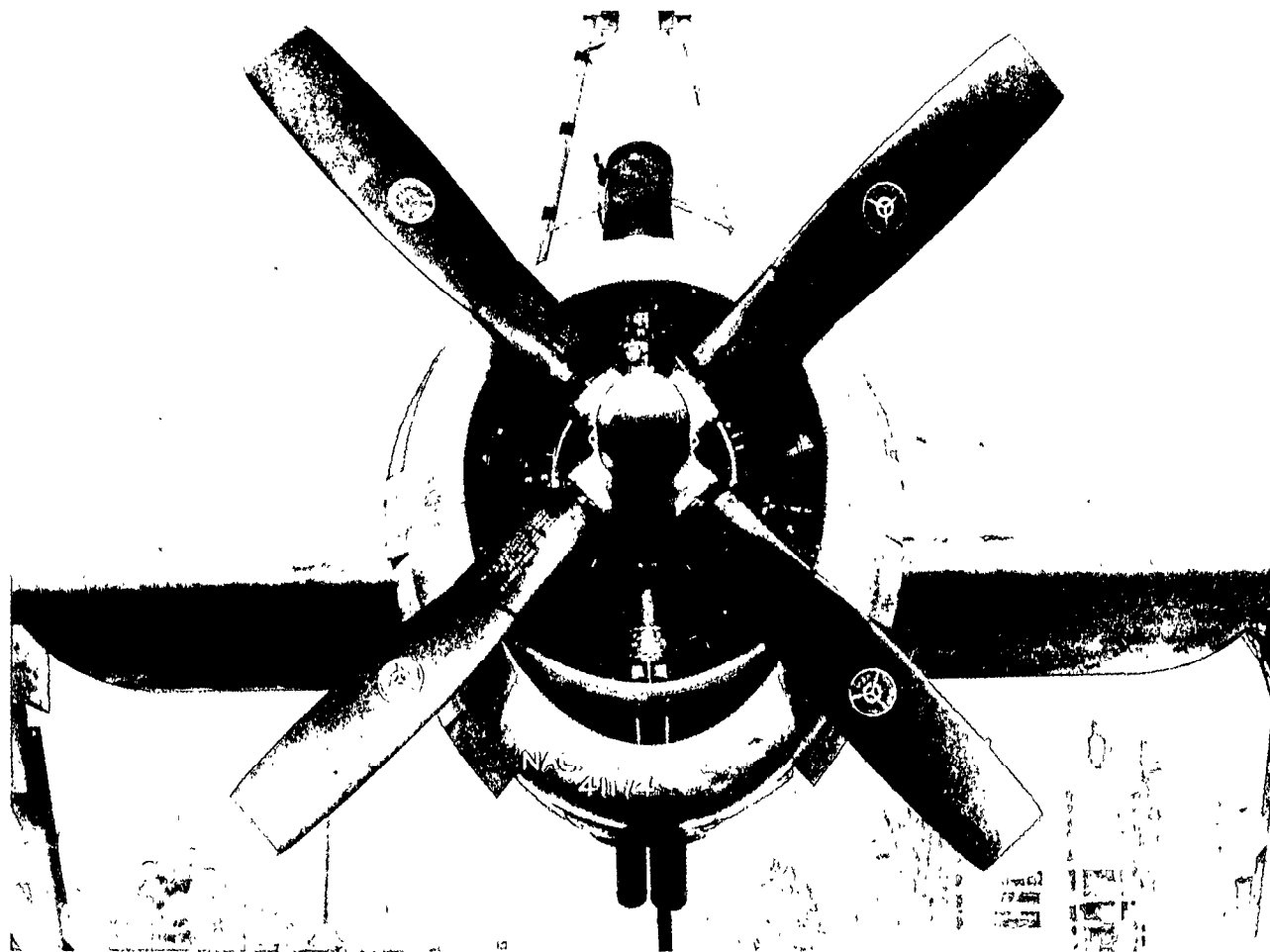
Figure 4. - Modified cuffs installed on Hamilton Standard hydraulic propeller.



(b) Side view.

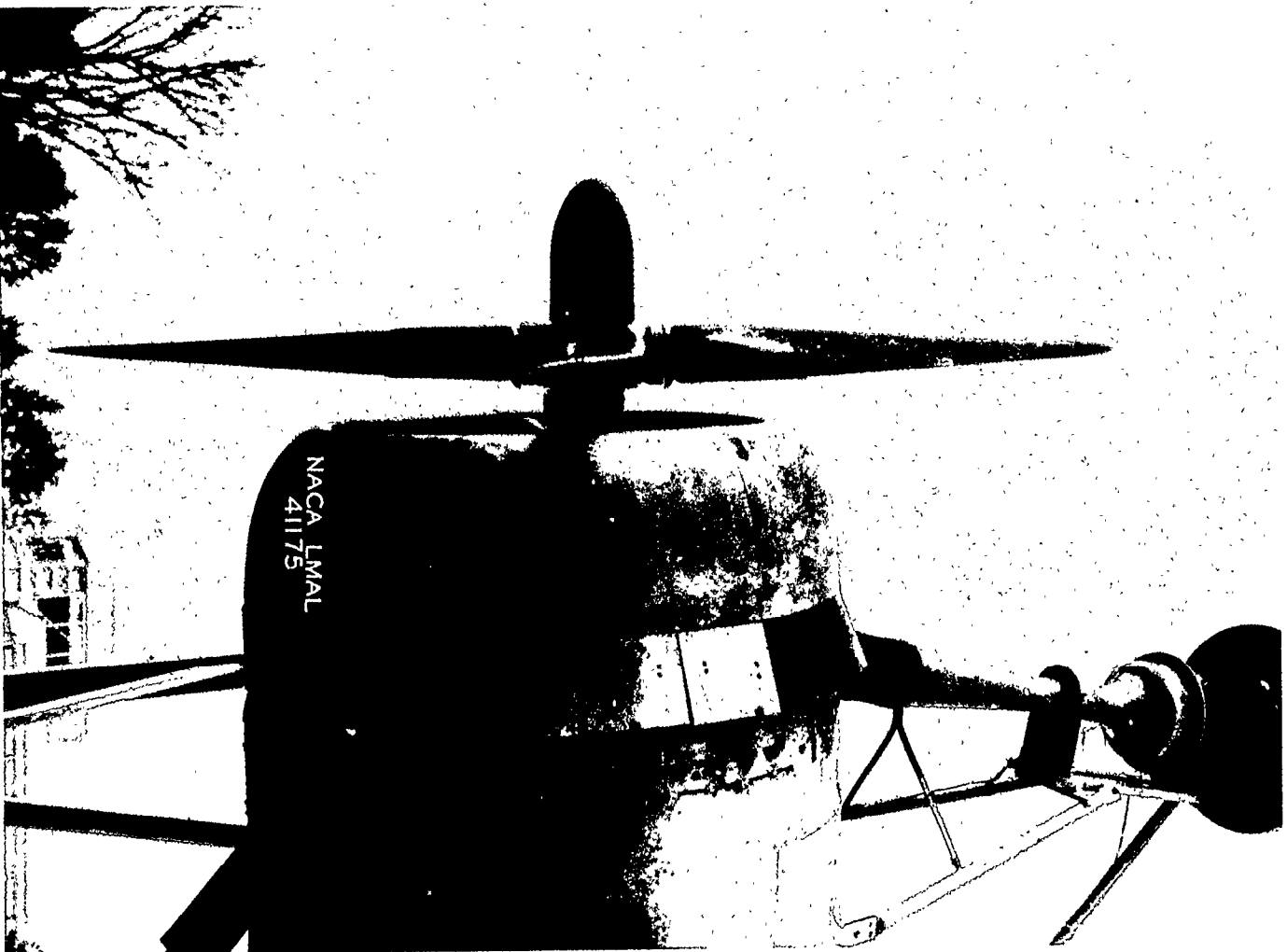
Figure 4.- Concluded.

NACA



(a) Front view.

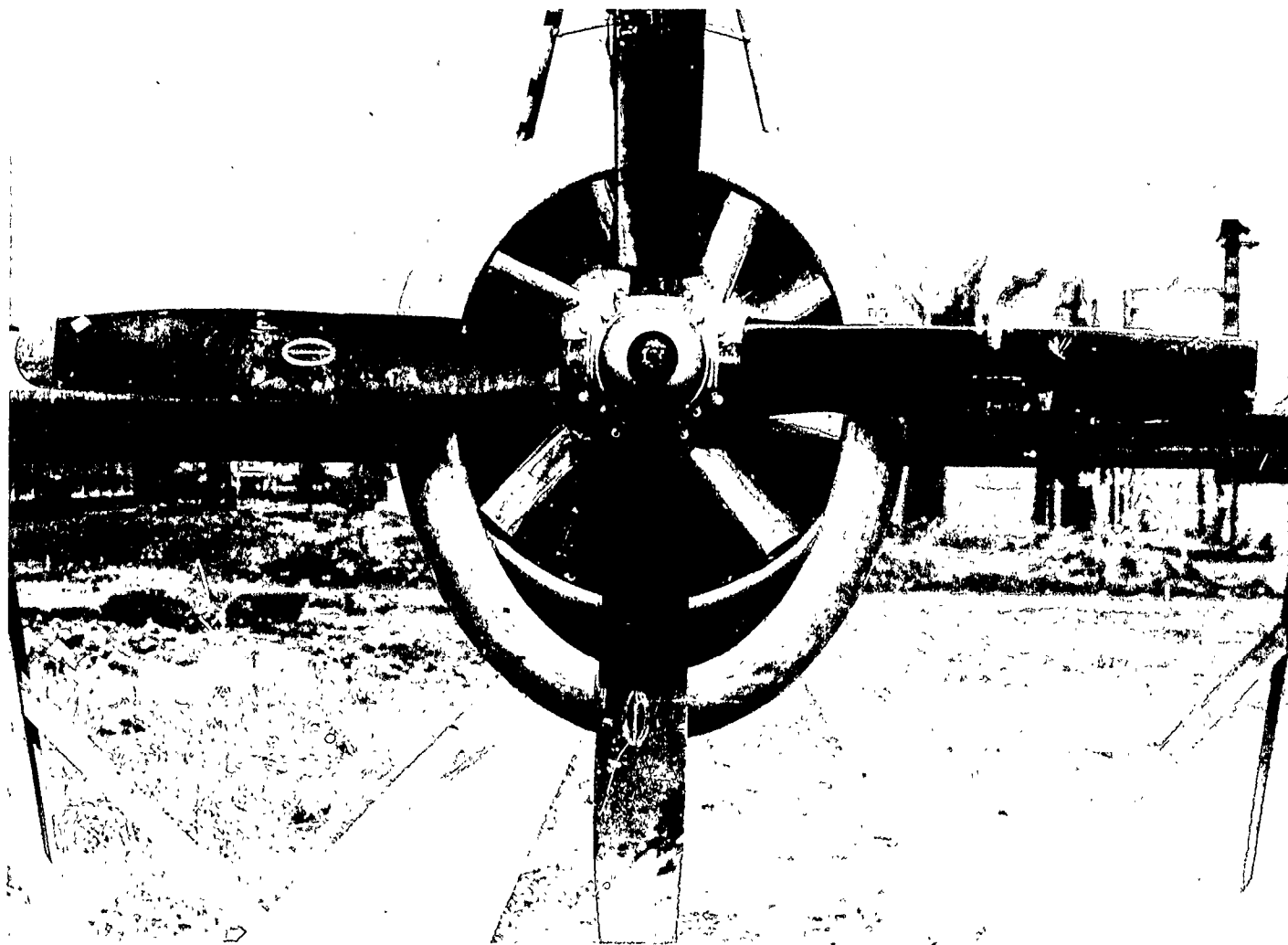
Figure 5.- Curtiss Electric propeller installed on model.



(b) Side view.

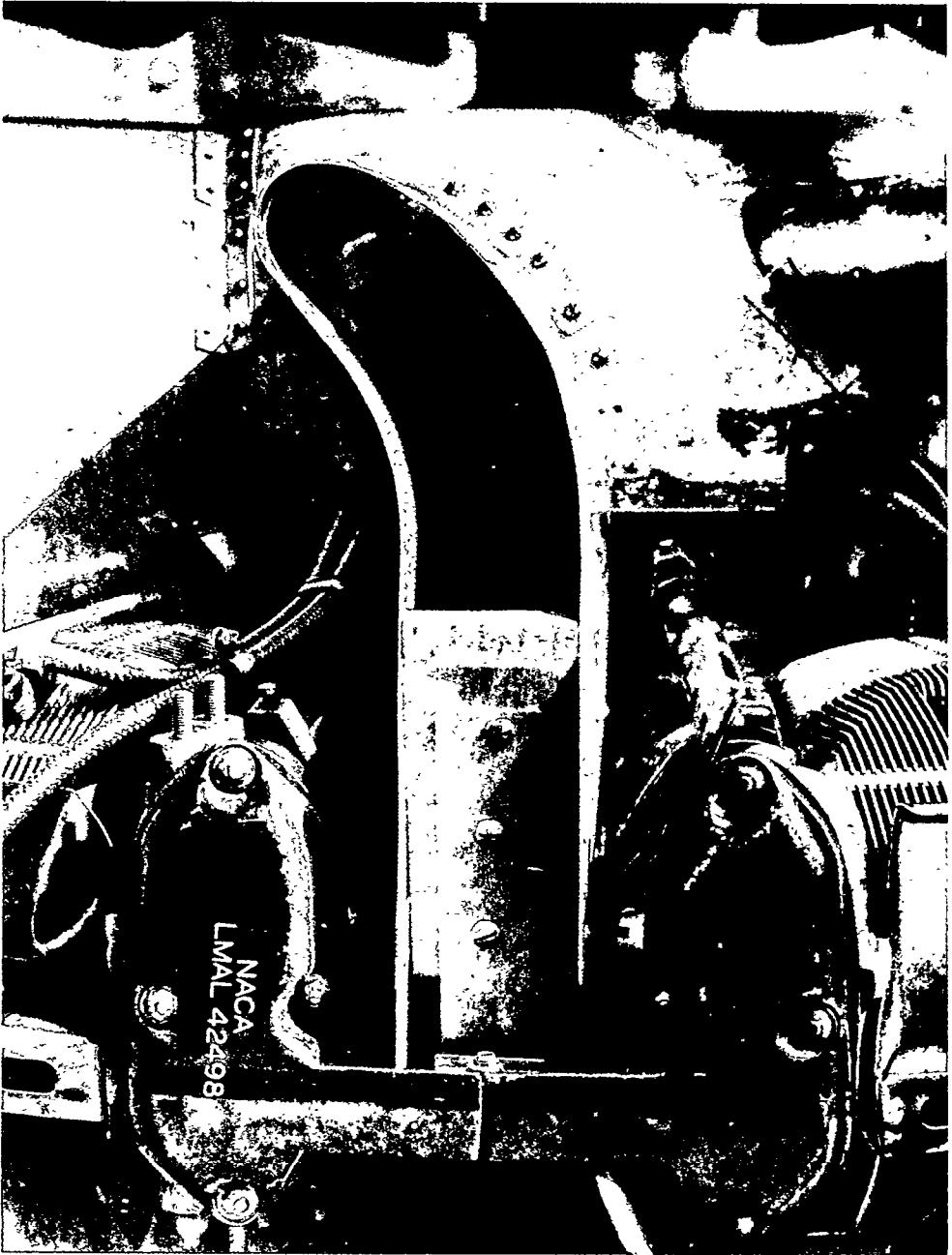
Figure 5. - Concluded.





(a) Front view.

Figure 6.- Guide vanes installed in cowling entrance.



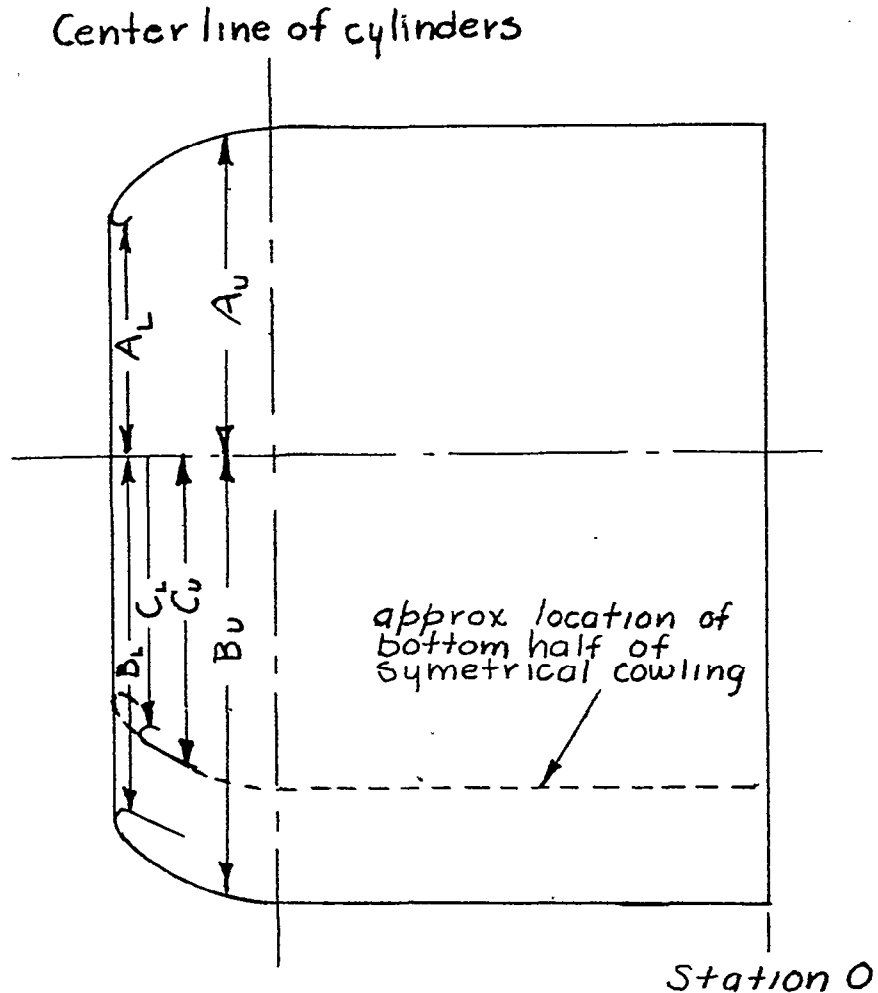
(b) Top view.

Figure 6. - Concluded.

NACA

NACA RM No. SL7110





Note: See table I for  
cowling coordinates



Figure 7.- External shapes ahead of fire wall for cowlings used.

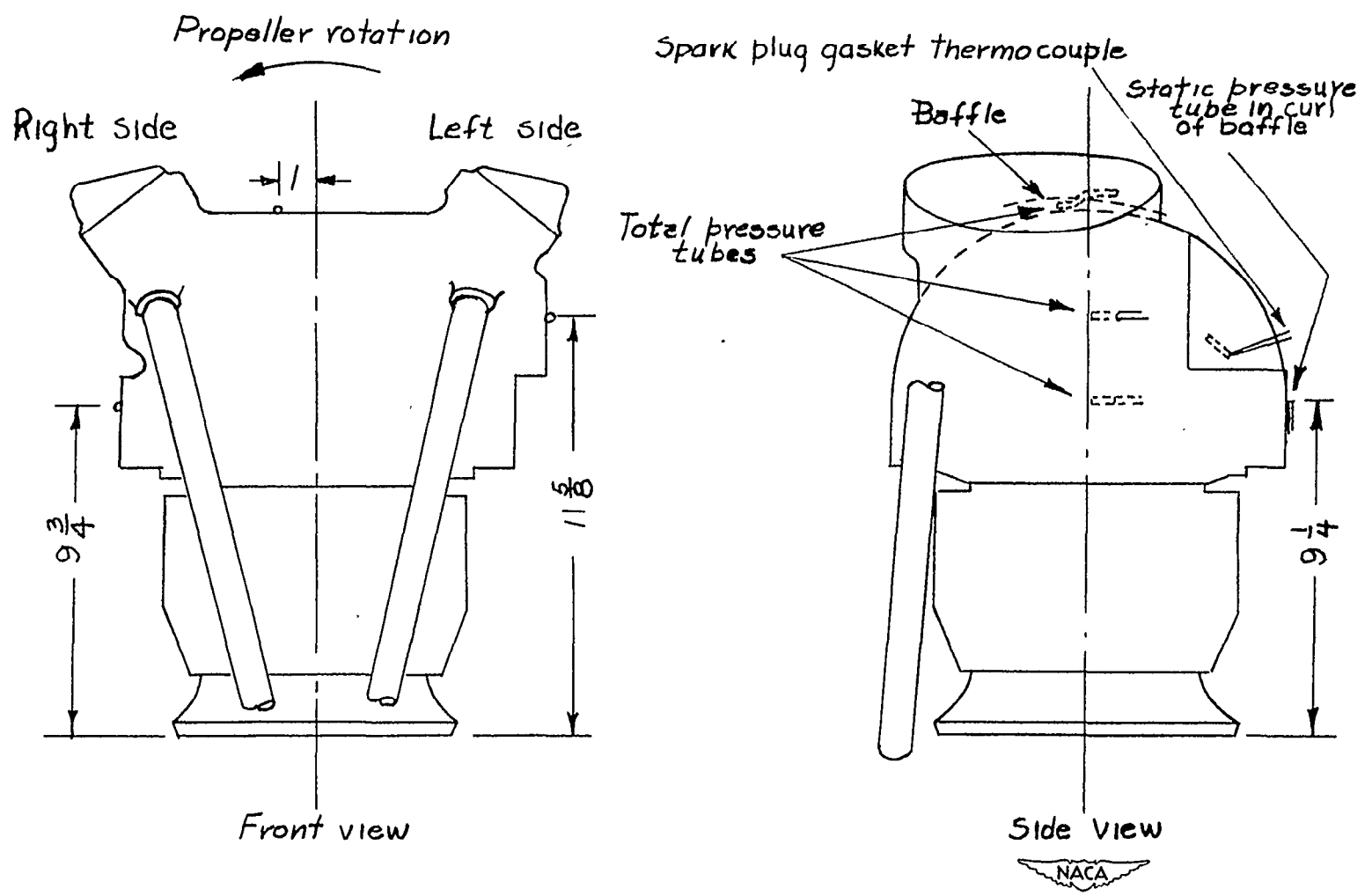


Figure 8.- Engine cylinder instrumentation.

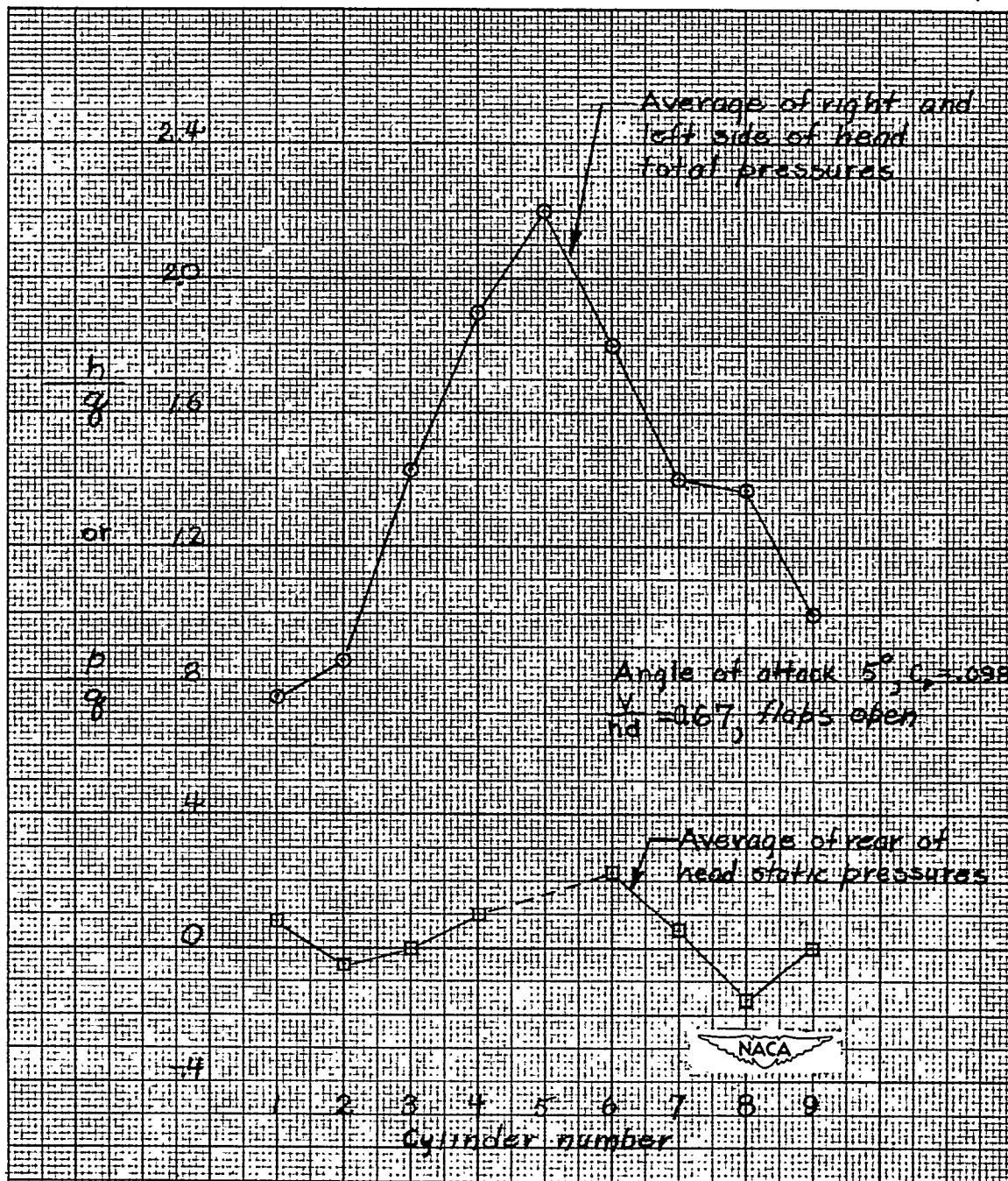
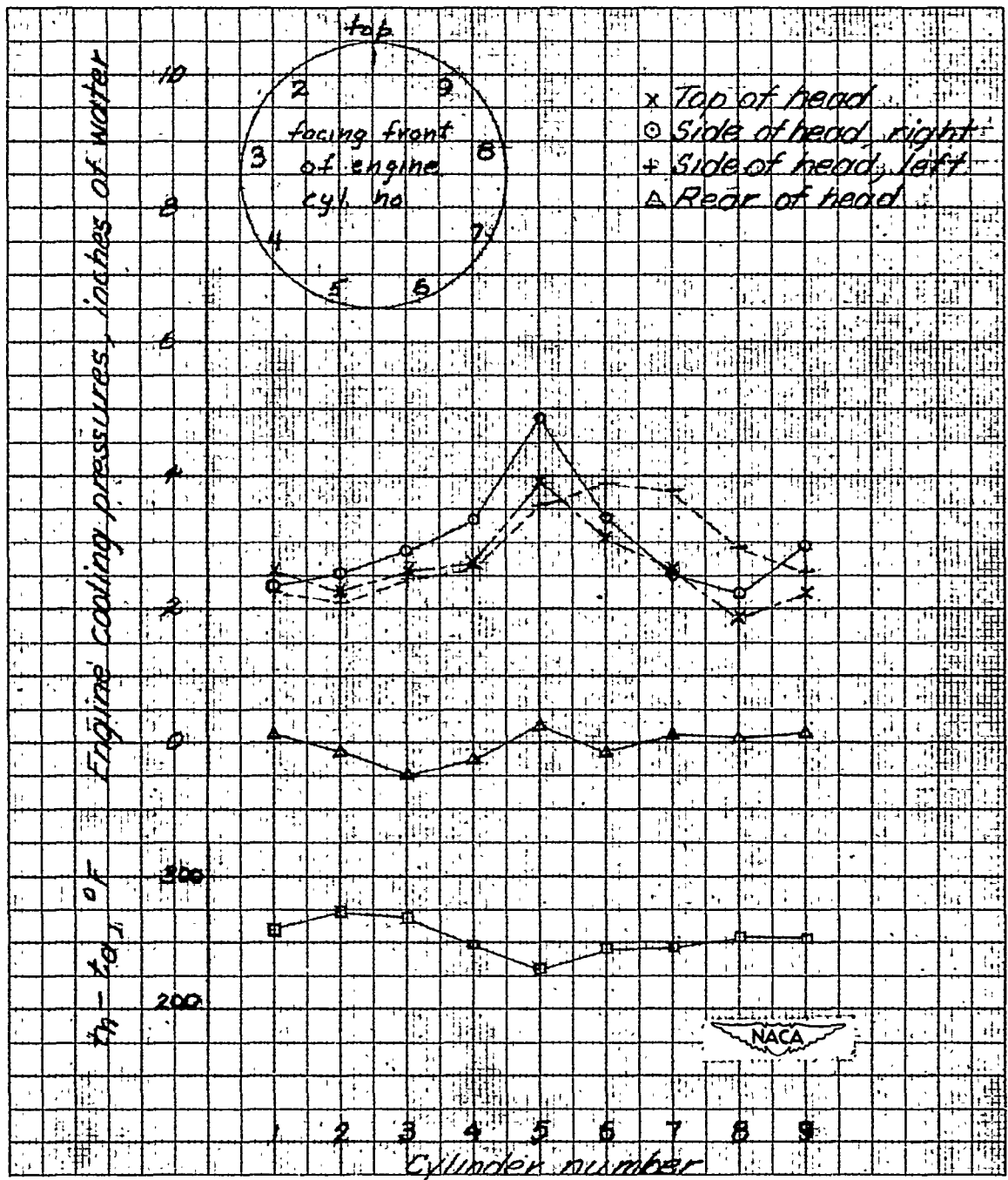
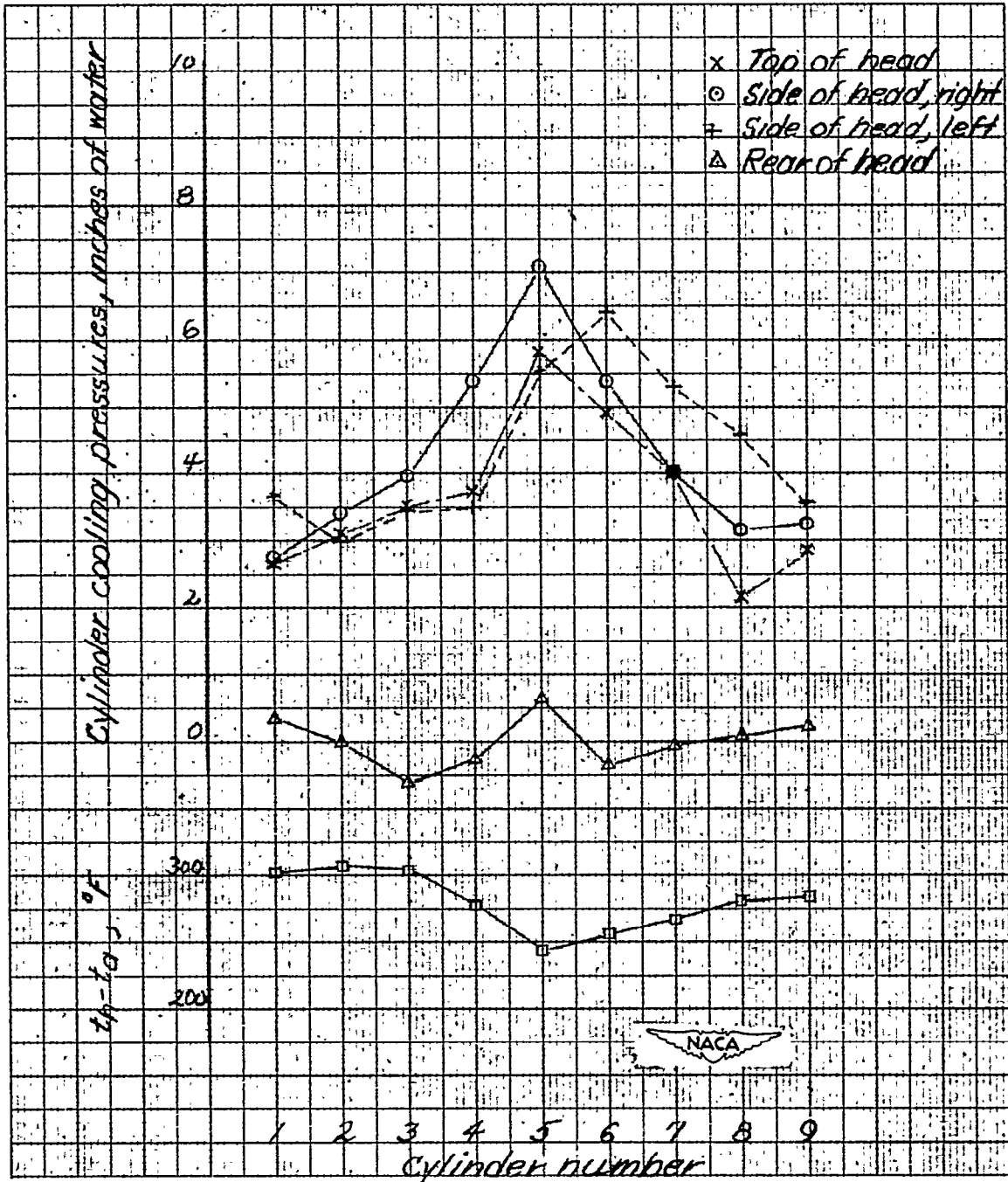


Figure 9.- Circumferential pressure distributions for underslung cowling with Hamilton Standard propeller as obtained in the wind-tunnel tests.



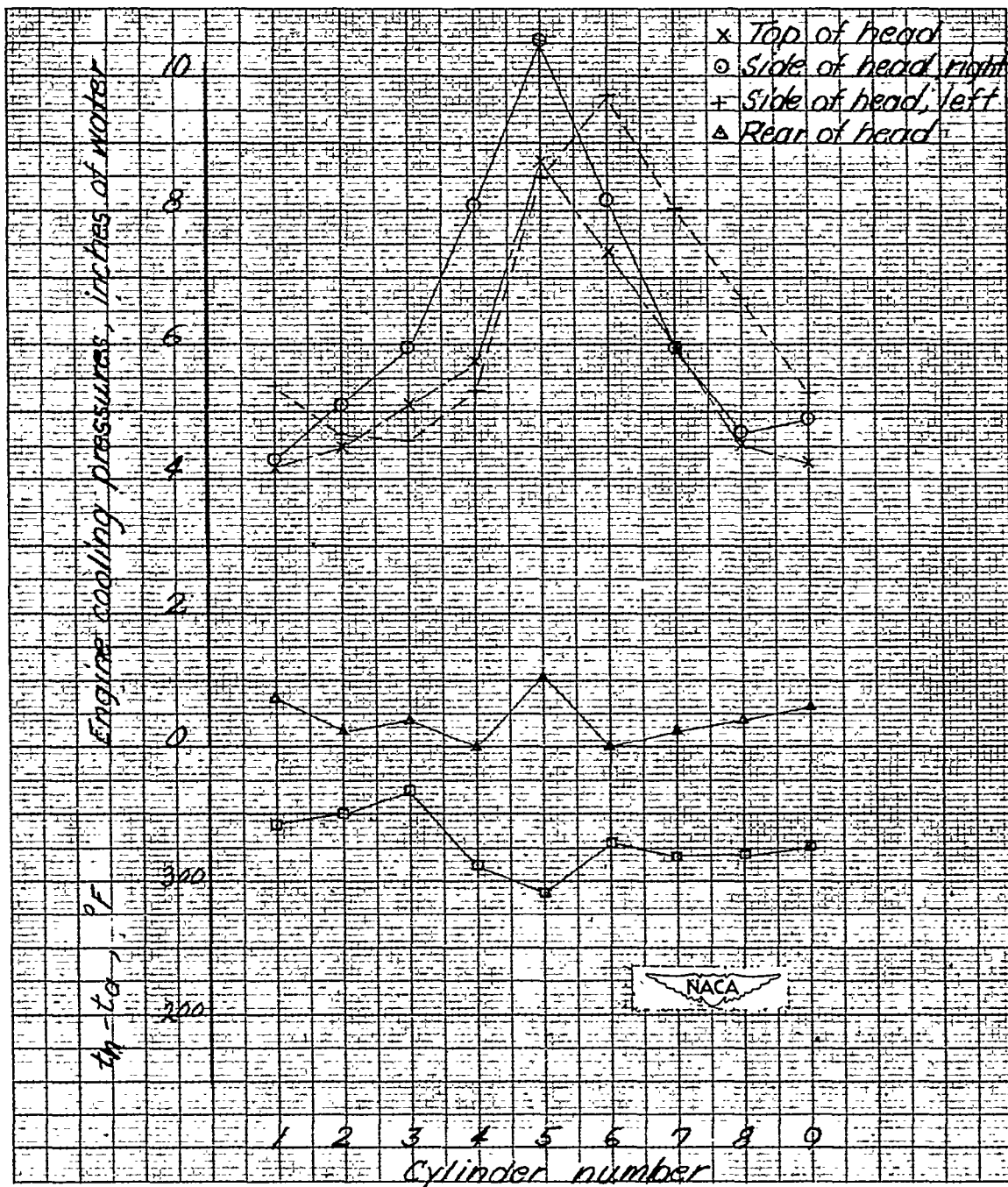
(a) 1630 rpm, 320 bhp.

Figure 10.- Engine pressure and temperature distributions for underslung cowling, Hamilton Standard propeller with normal cuffs and cowling flaps full open.  $C_p = 0.125$ .



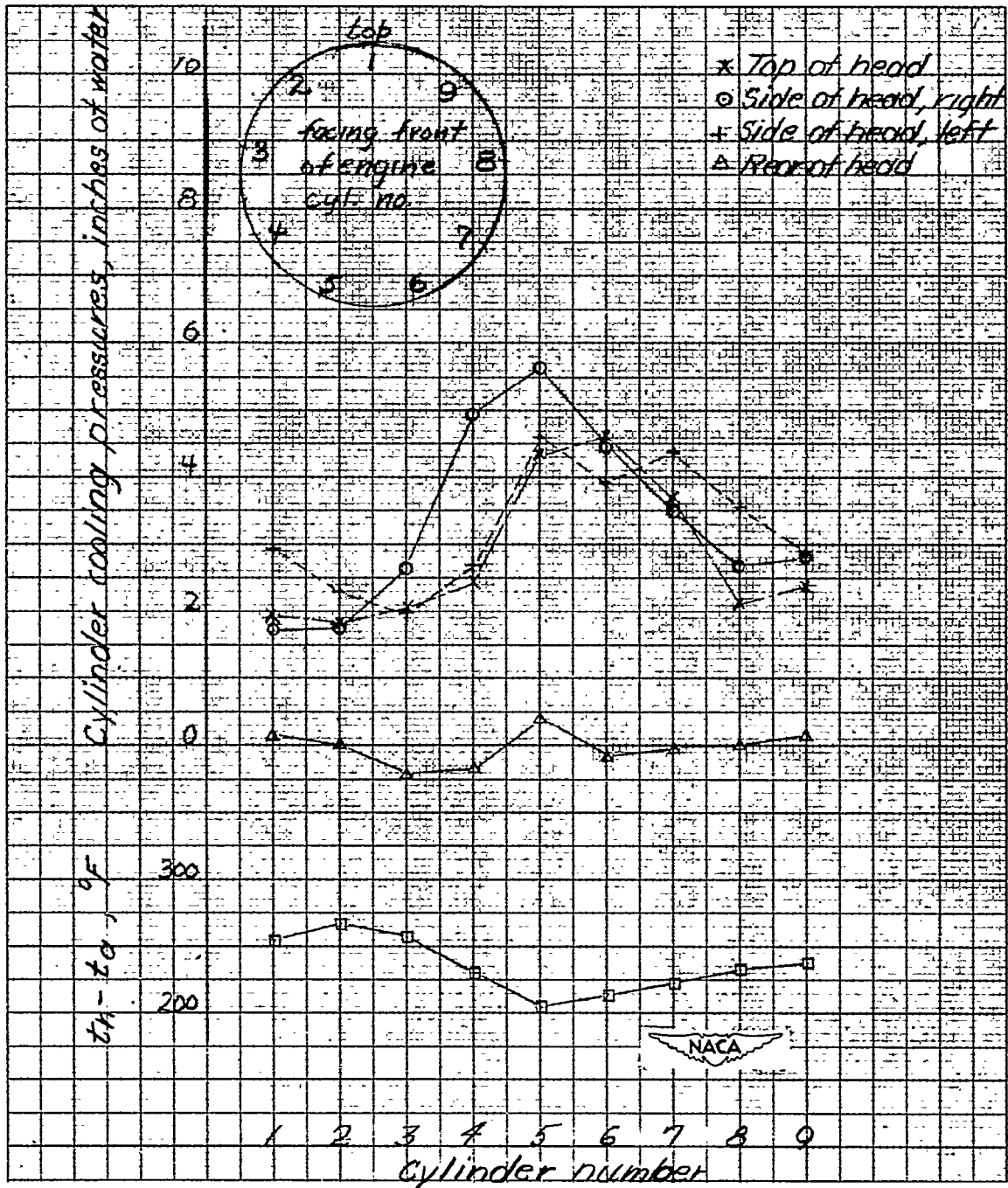
(b) 1940 rpm, 550 bhp.

Figure 10.- Continued.



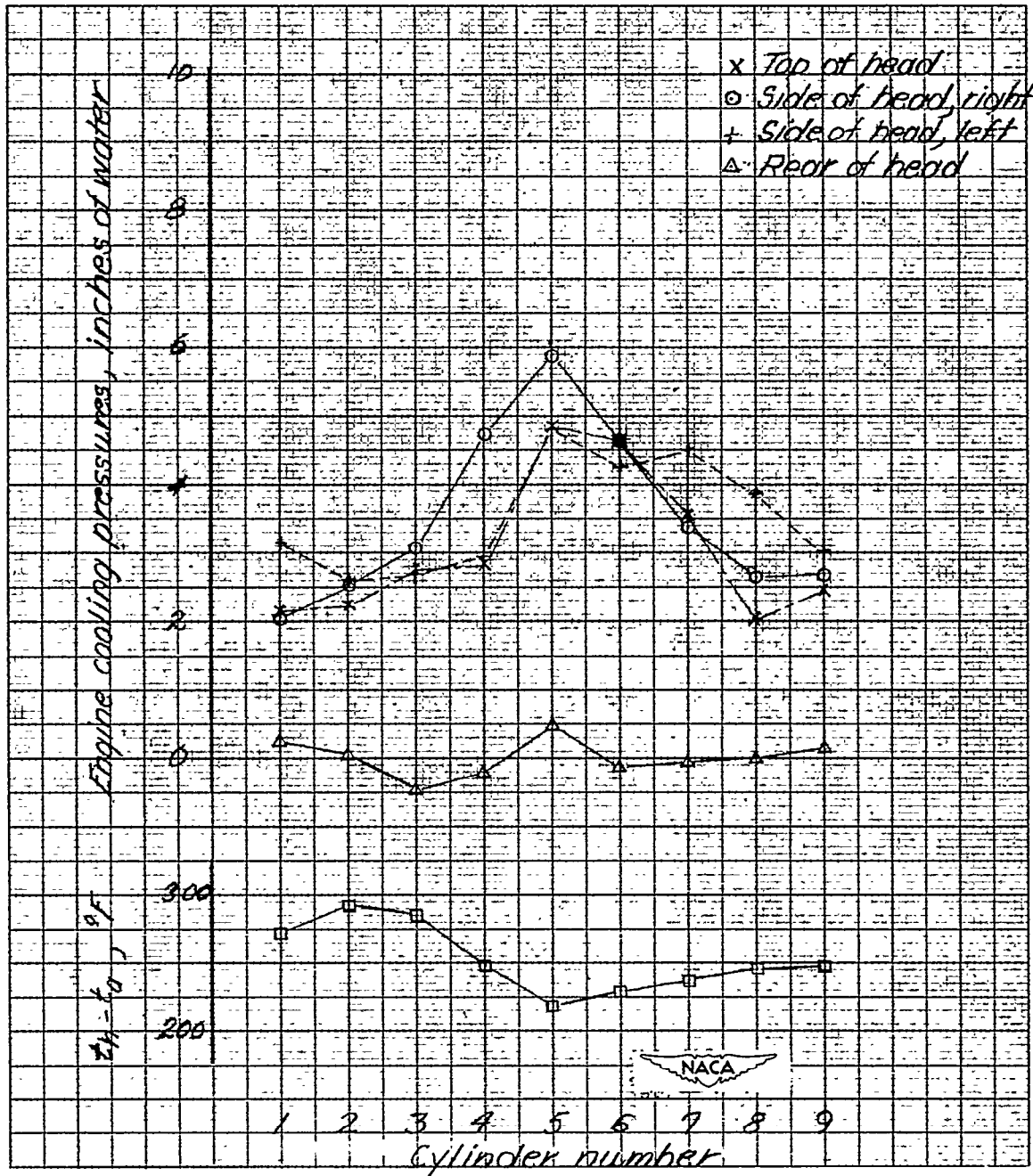
(c) 2400 rpm, 1040 bhp.

Figure 10.- Concluded.



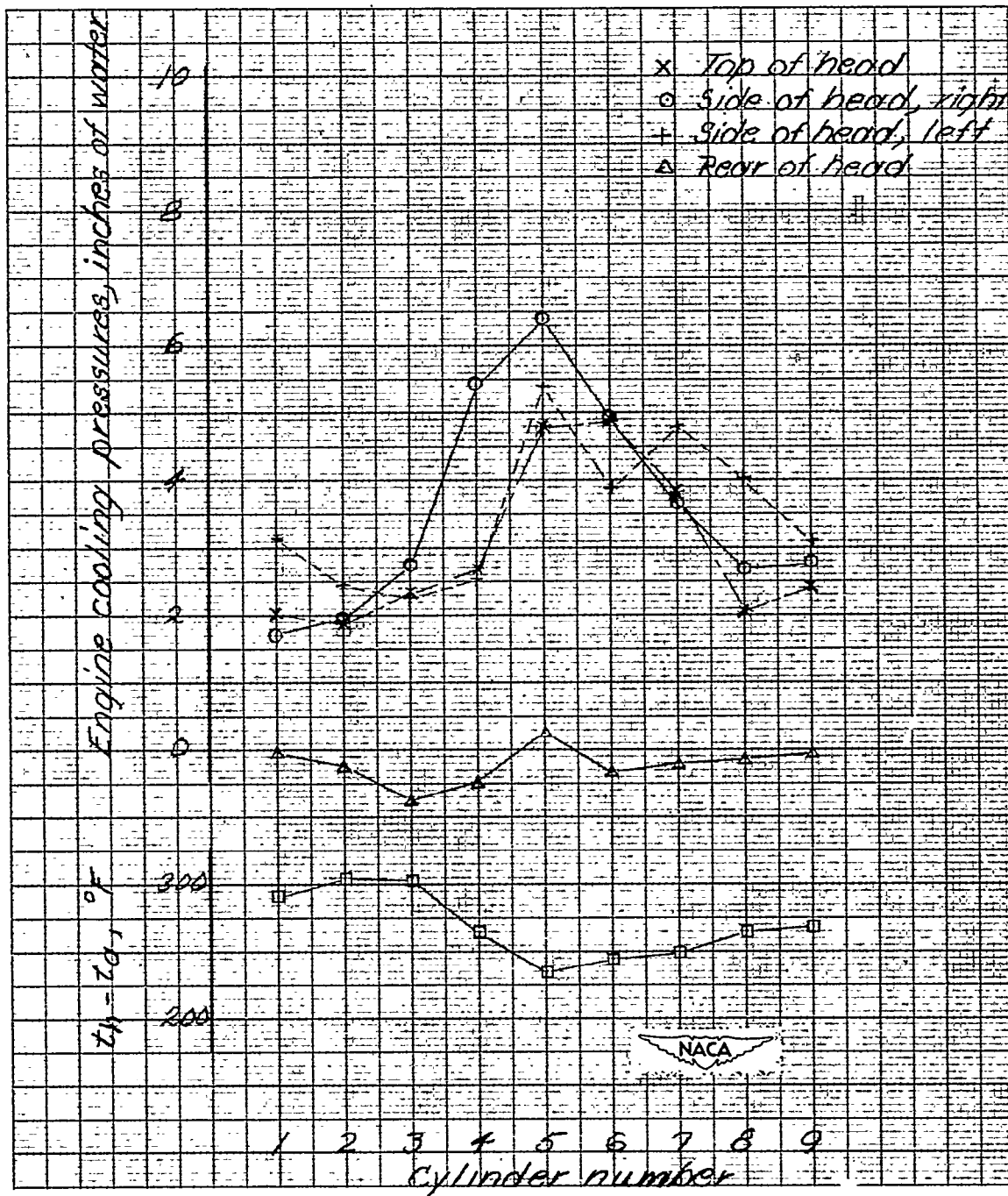
(a) 1800 rpm, 300 bhp,  $C_D = 0.08$ .

Figure 11.- Engine pressure and temperature distributions for under-slung cowling, Hamilton Standard propeller, with normal cuffs and cowling flaps full open.



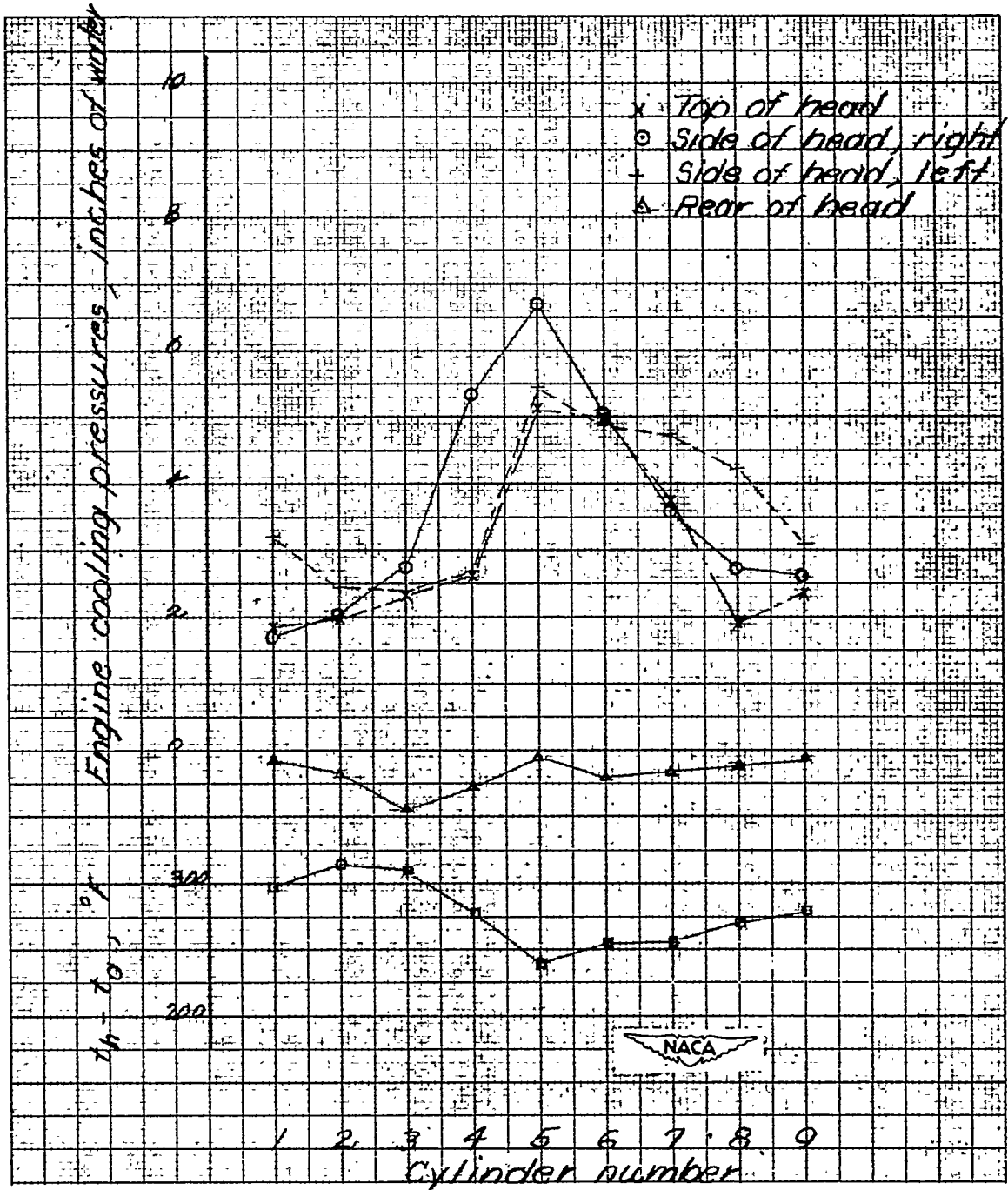
(b) 1800 rpm, 400 bhp,  $C_P = 0.11$ .

Figure 11.- Continued.



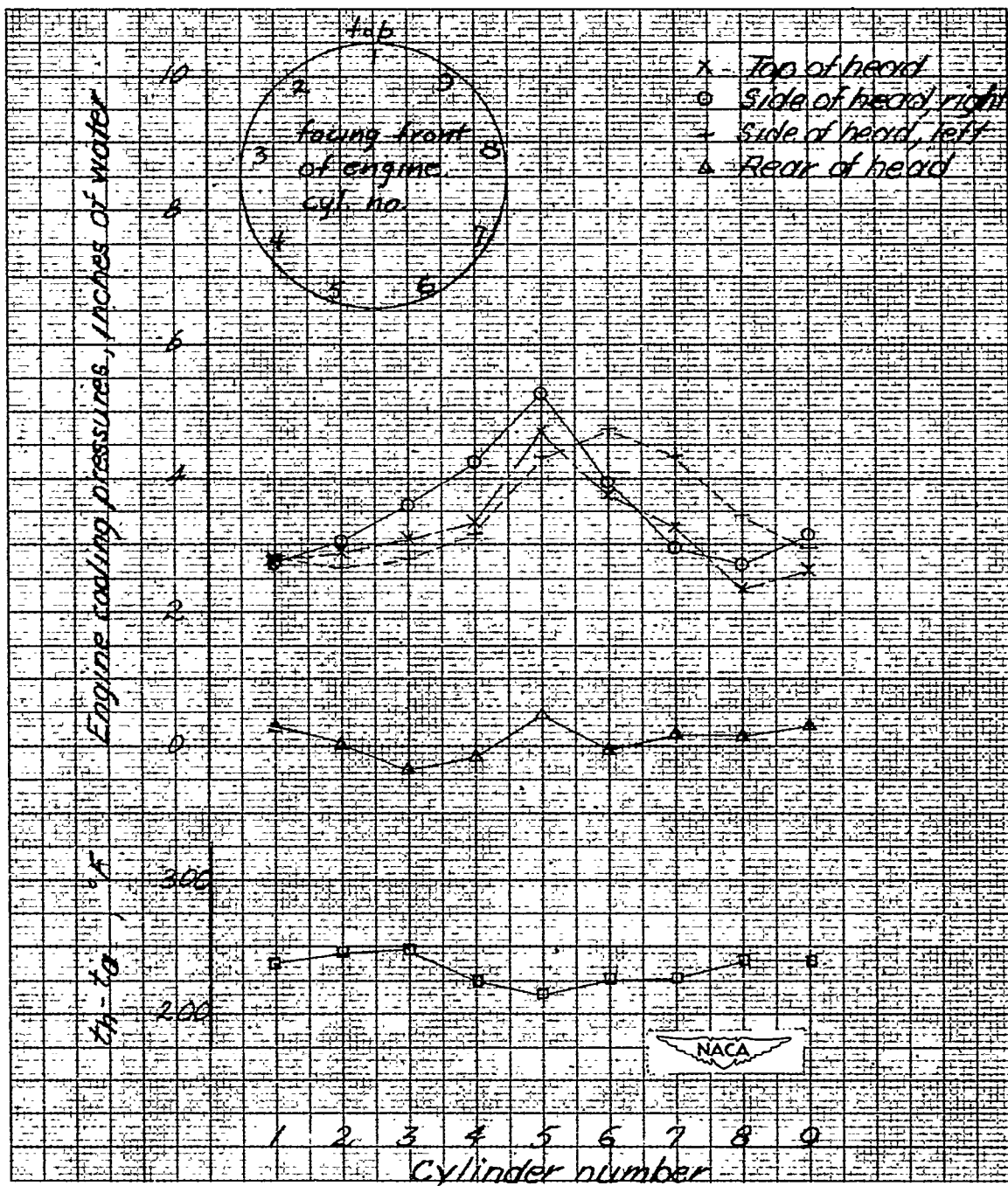
(c) 1800 rpm, 500 bhp,  $C_P = 0.13$ .

Figure 11.- Continued.



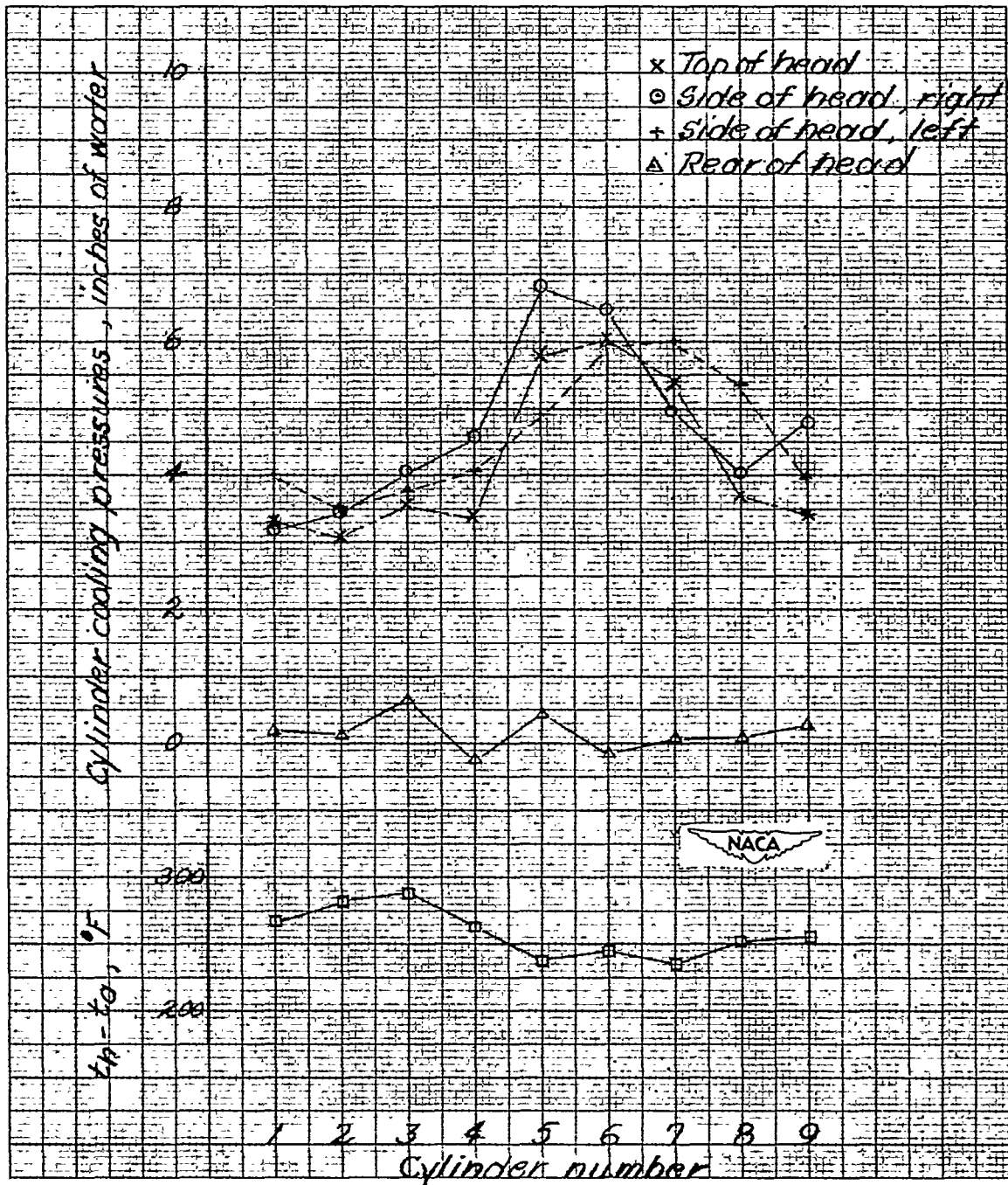
(d) 1800 rpm, 600 bhp,  $C_D = 0.16$ .

Figure 11.- Concluded.



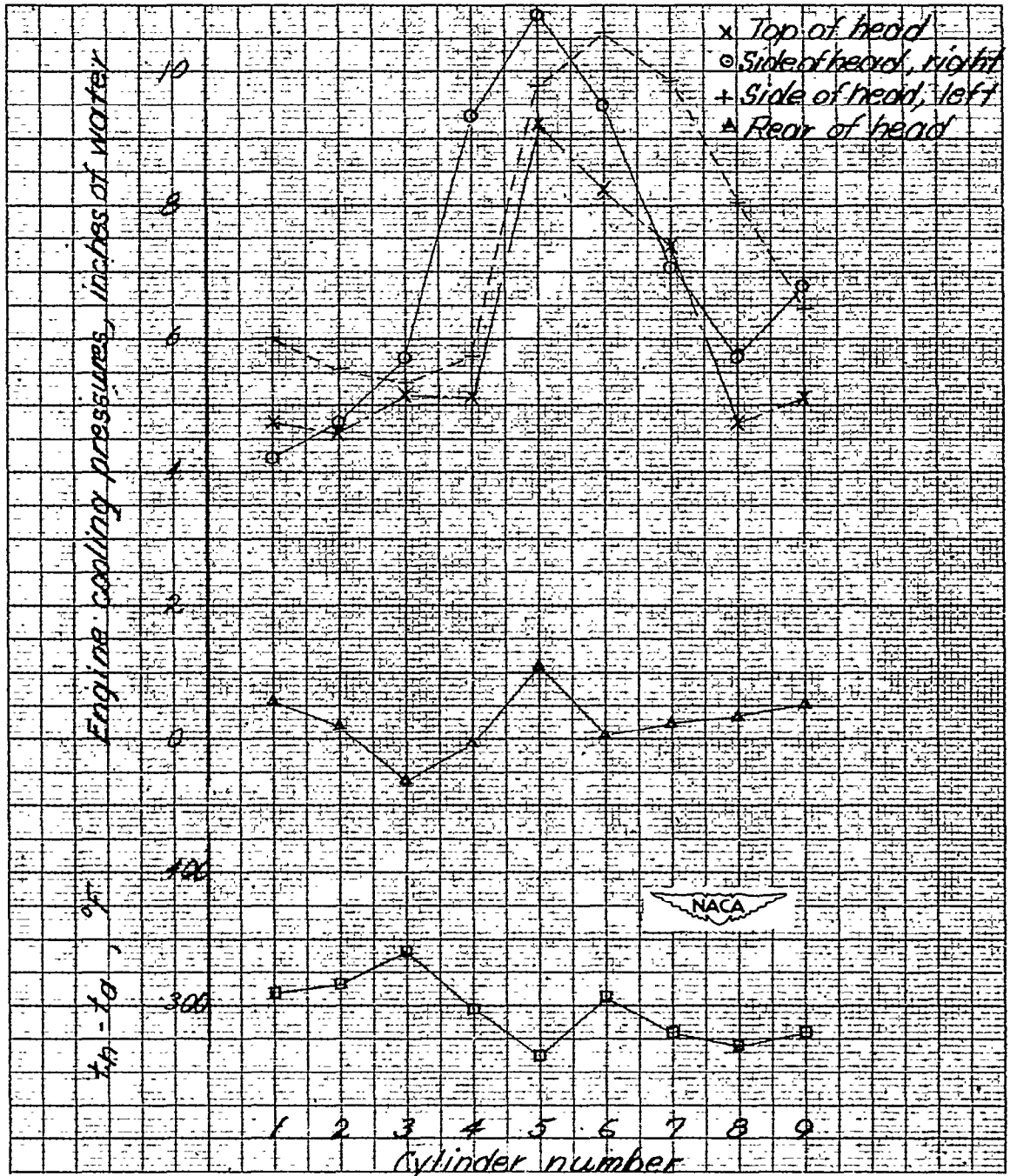
(a) 1630 rpm, 320 bhp.

Figure 12.- Engine pressure and temperature distributions for underslung cowling, Hamilton Standard propeller with modified cuffs and cowling flaps full open.  $C_D = 0.125$ .



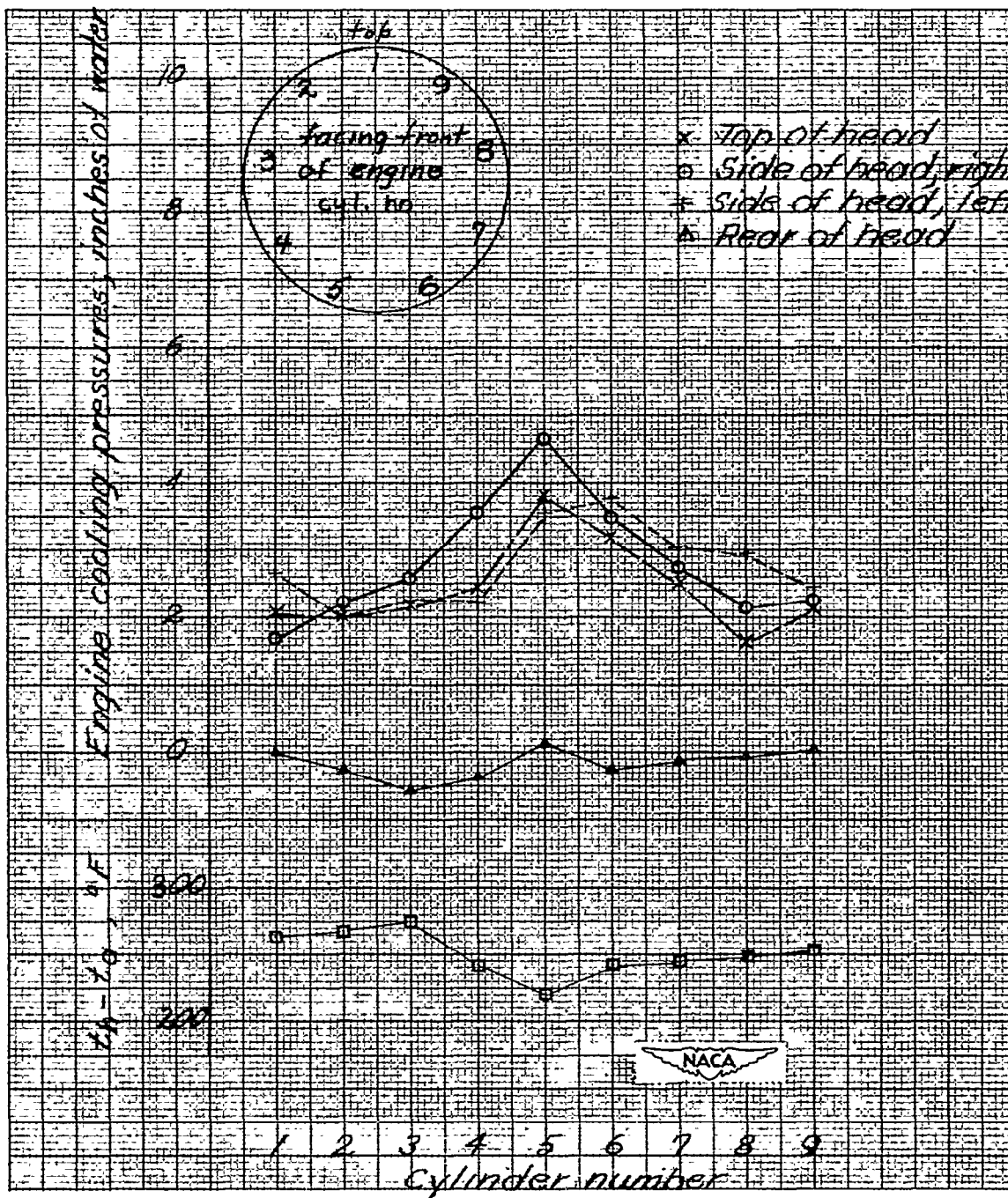
(b) 1940 rpm, 550 bhp.

Figure 12.- Continued.



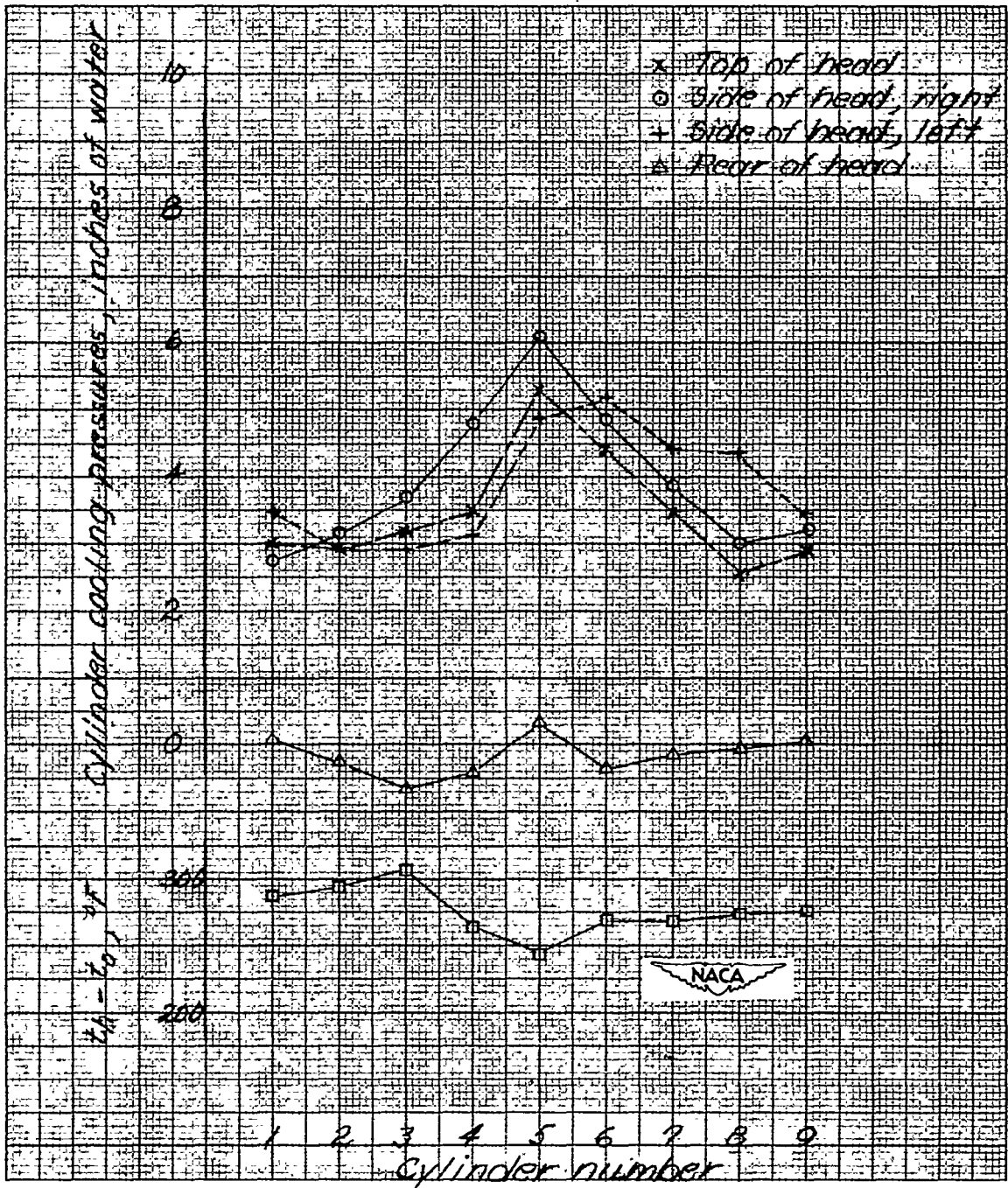
(c) 2400 rpm, 1040 bhp.

Figure 12.- Concluded.



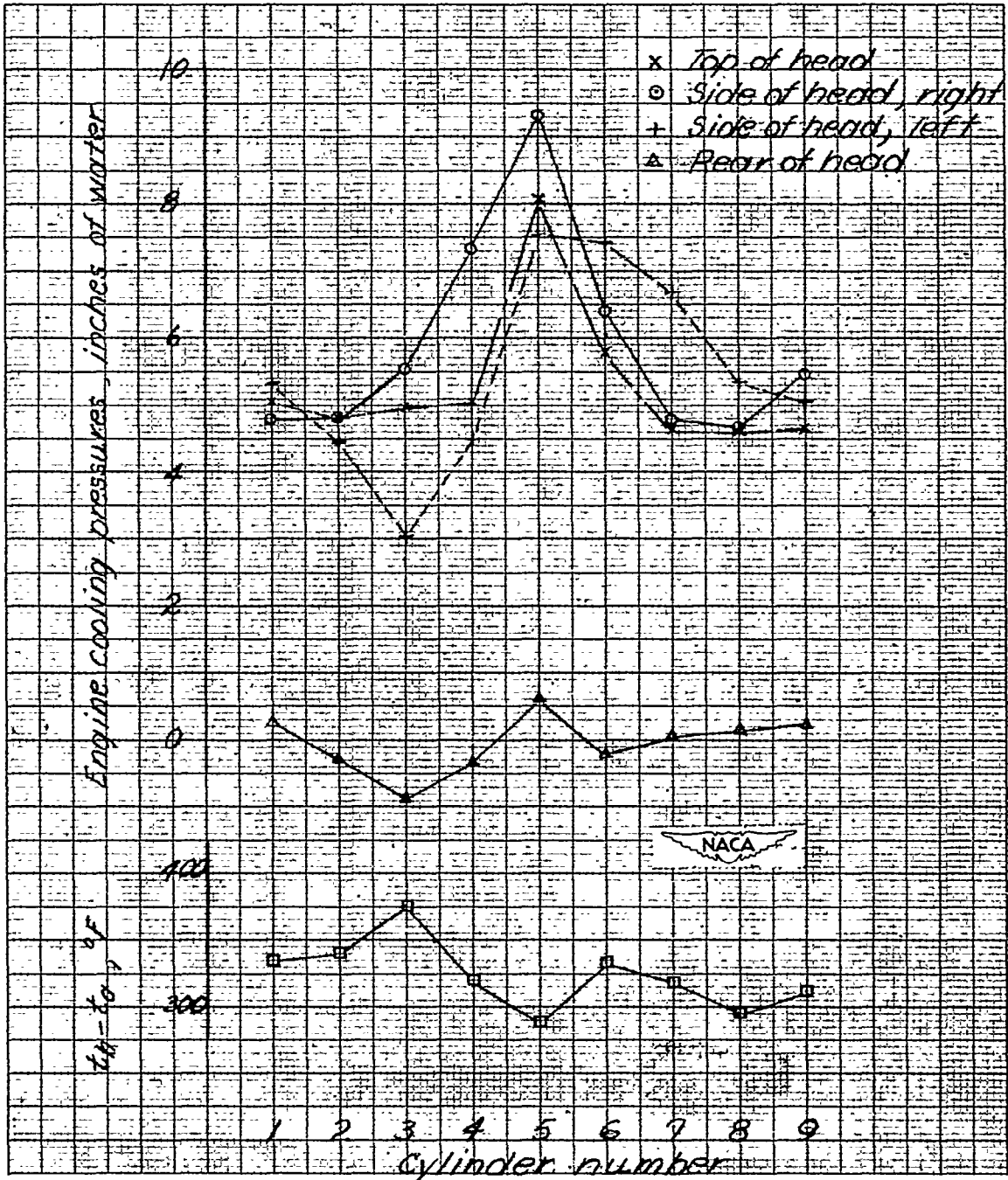
(a) 1630 rpm, 320 bhp.

Figure 13.- Engine pressure and temperature distributions for under-slung cowling, Curtiss Electric propeller and cowling flaps full open.  $C_p = 0.125$ .



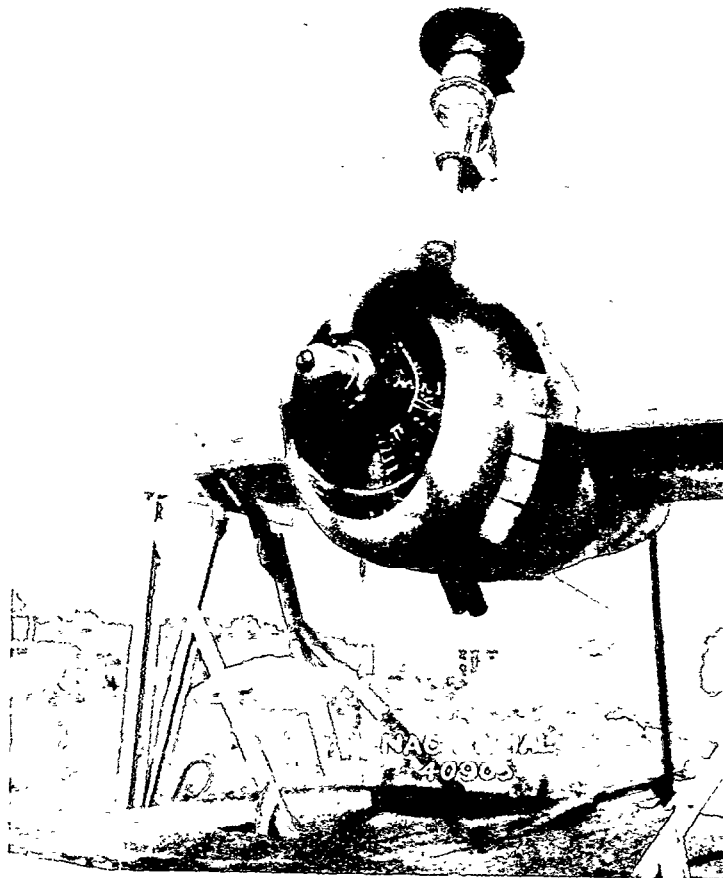
(b) 1940 rpm, 550 bhp.

Figure 13.- Continued.



(c) 2400 rpm, 1040 bhp.

Figure 13.- Concluded.



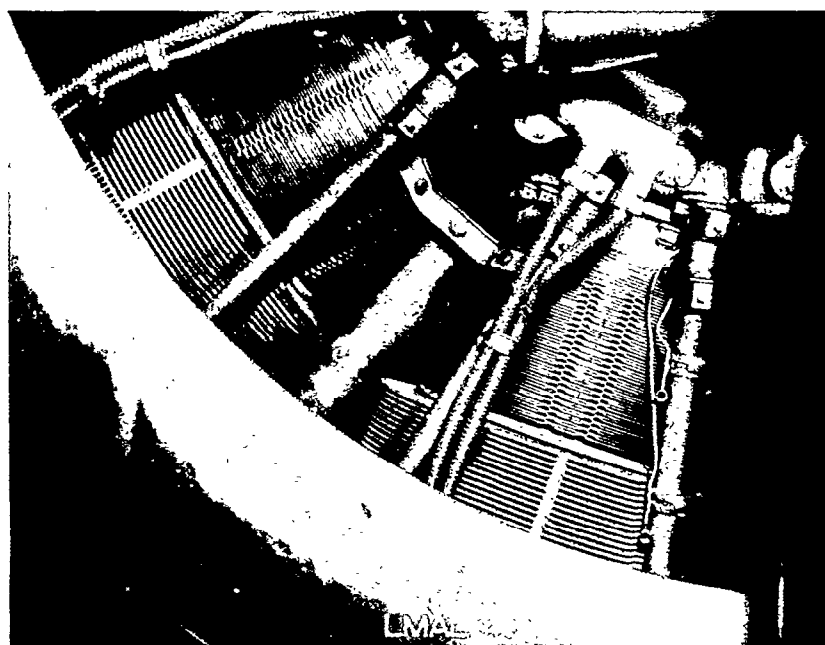
(a) Tufts at the cowling entrance.

Figure 14.- Flow studies of air direction in the cowling entrance and at the face of the engine by means of tufts and aluminum powder deposits.



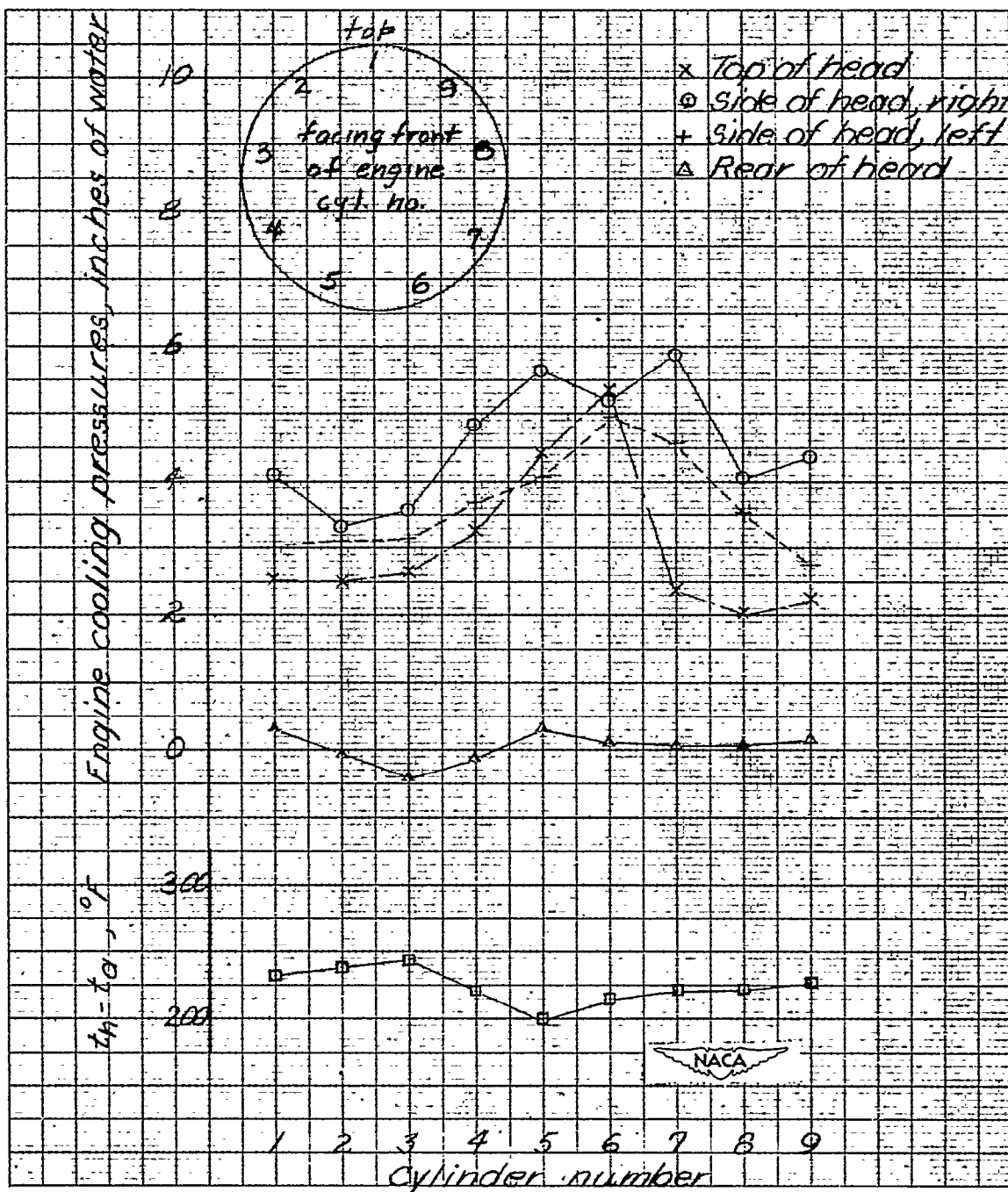
(b) Looking at face of engine against air rotation.

Figure 14.- Continued.



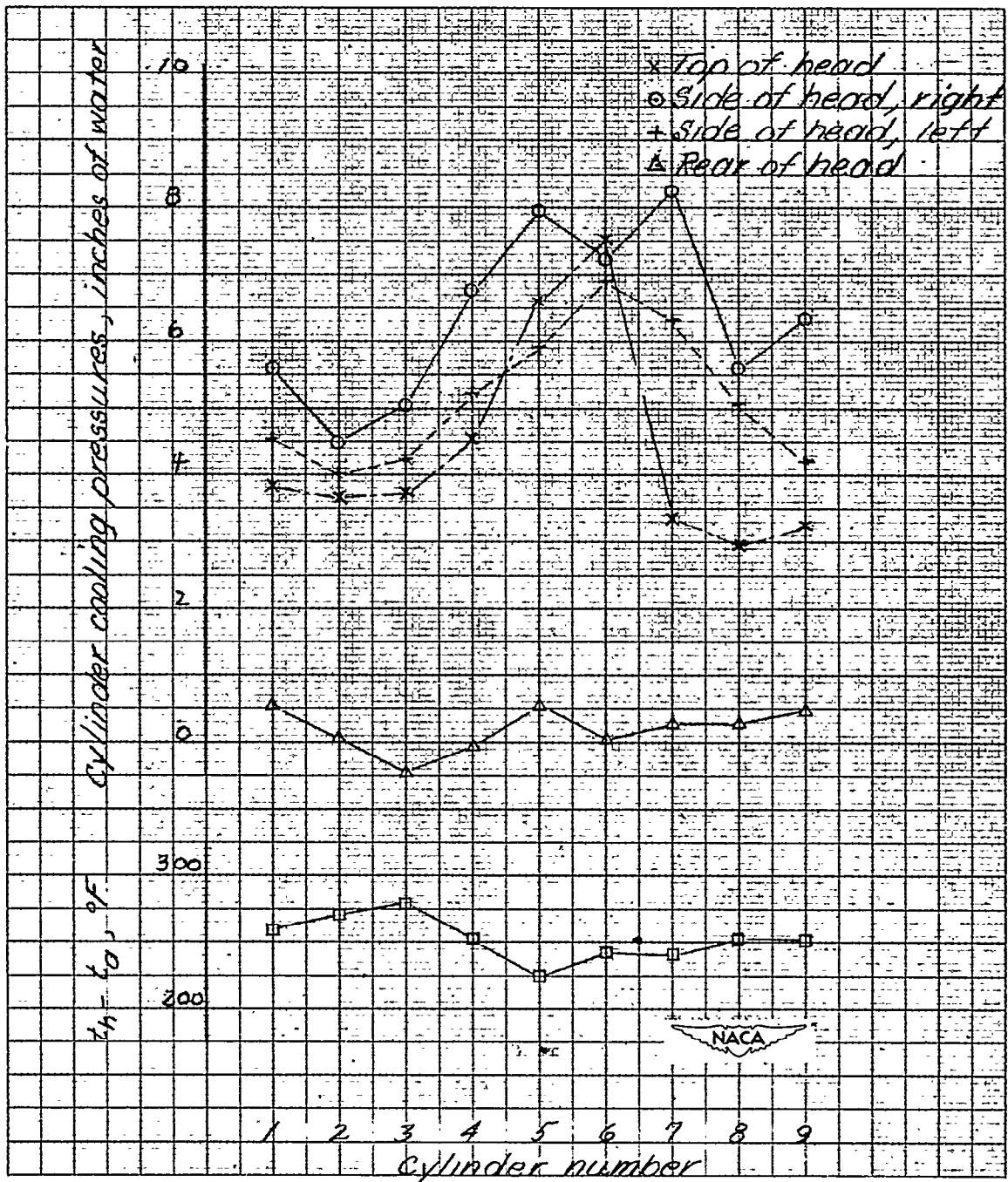
(c) Looking at face of engine parallel to propeller axis.

Figure 14.- Concluded.



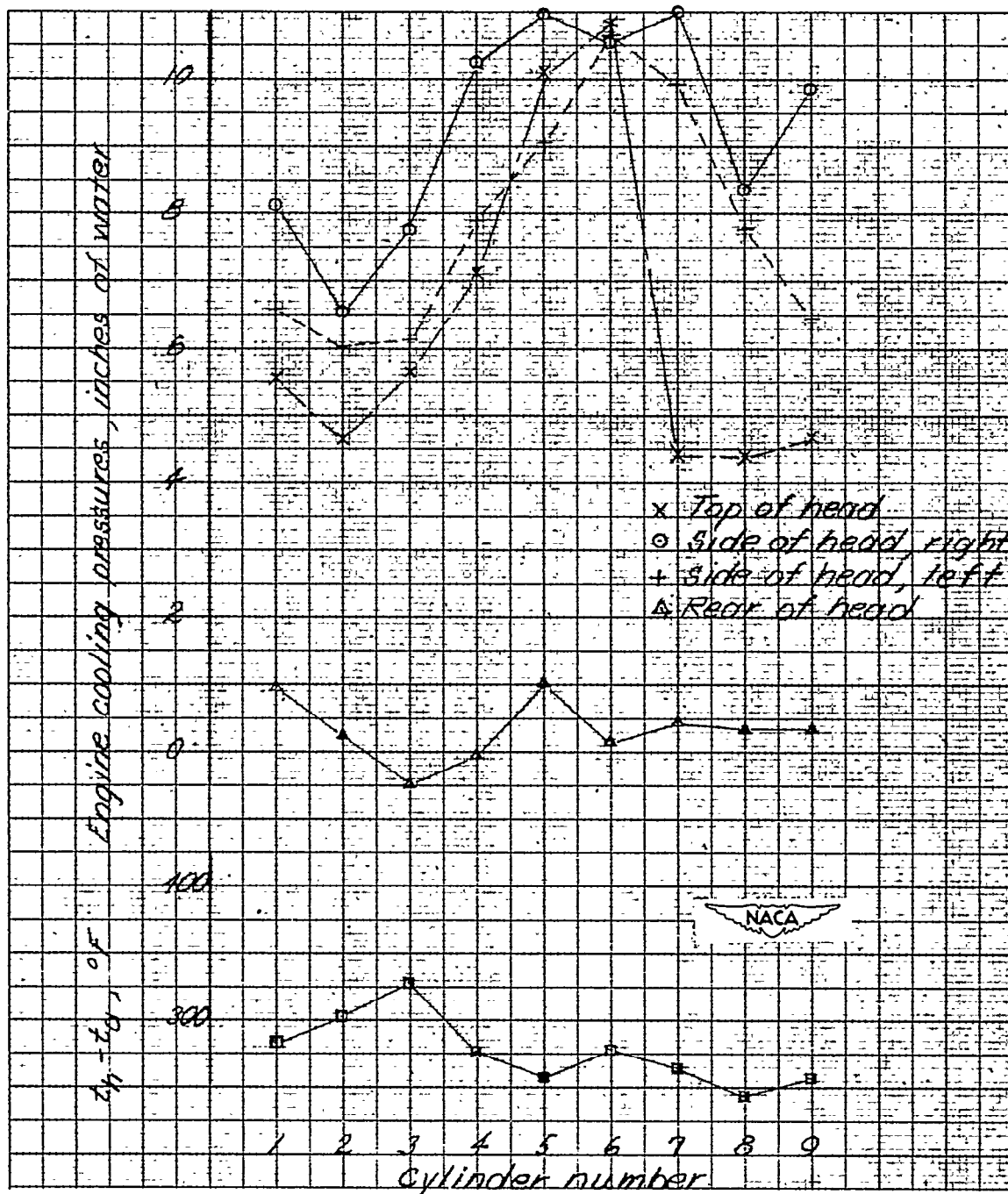
(a) 1630 rpm, 320 bhp.

Figure 15.- Engine pressure and temperature distributions for under-slung cowling, Hamilton Standard propeller with modified cuffs and vanes installed in cowling entrance, cowling flaps full open.  
 $C_P = 0.125$ .



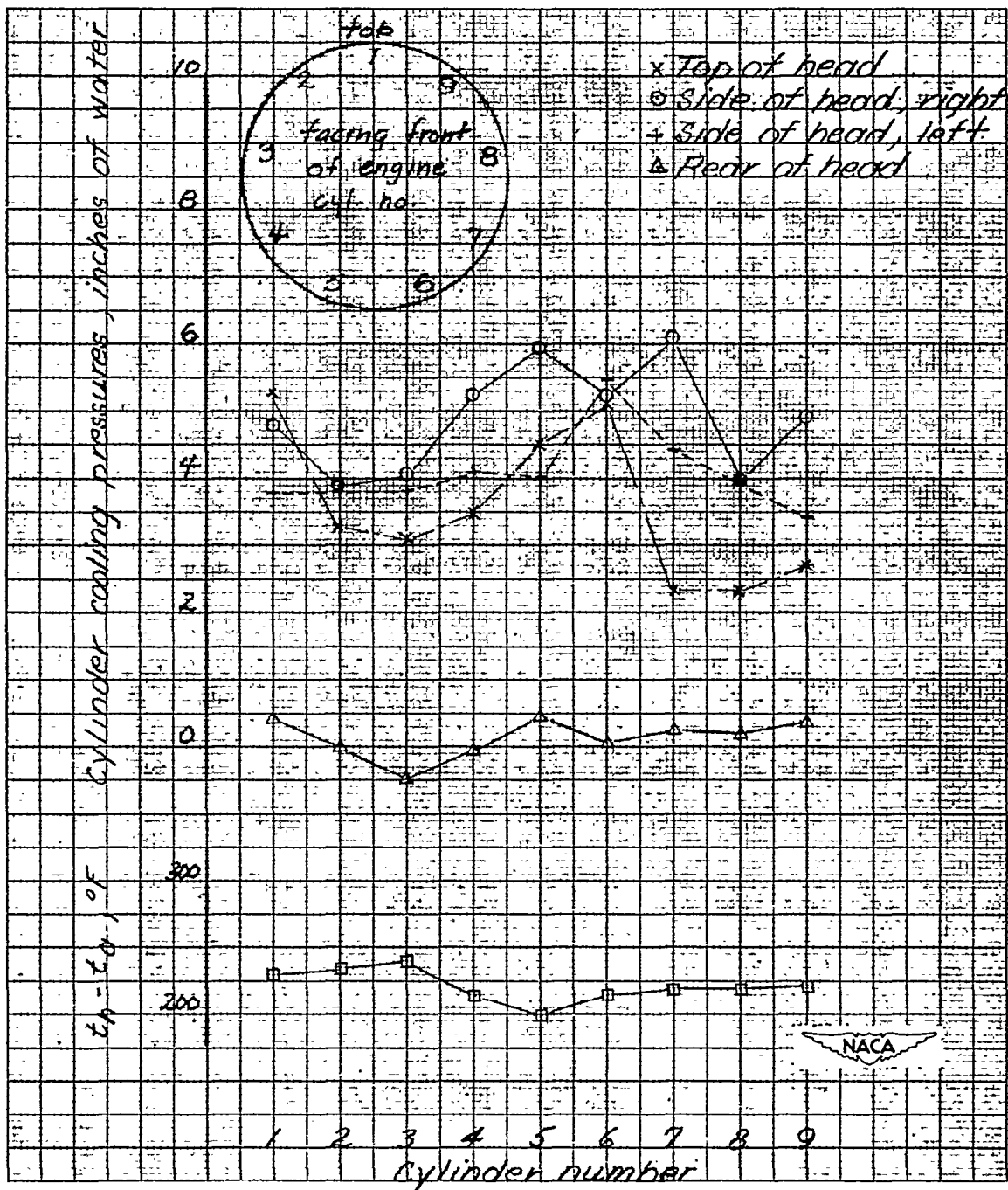
(b) 1940 rpm, 550 bhp.

Figure 15.- Continued.



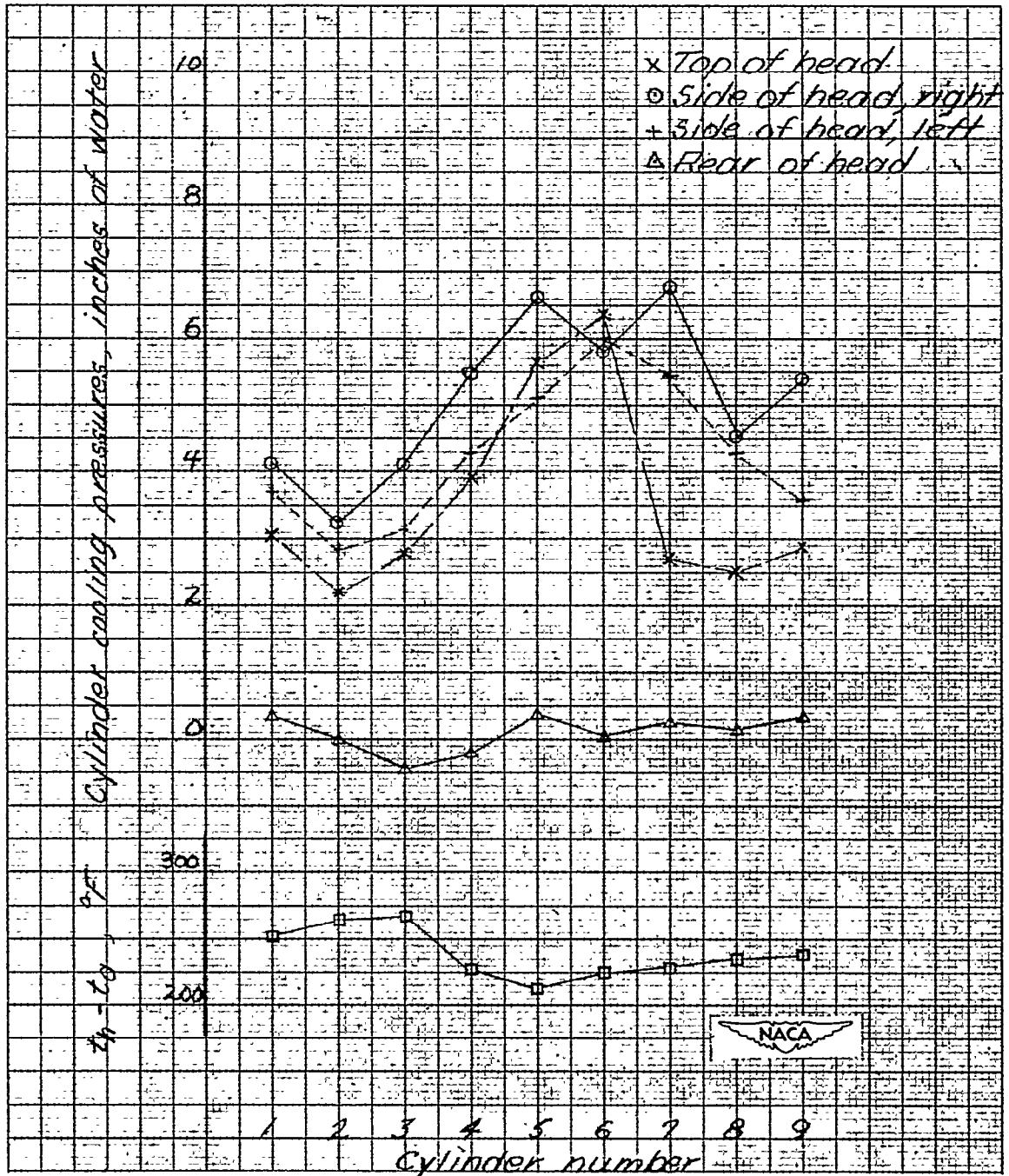
(c) 2400 rpm, 1040 bhp.

Figure 15.- Concluded.



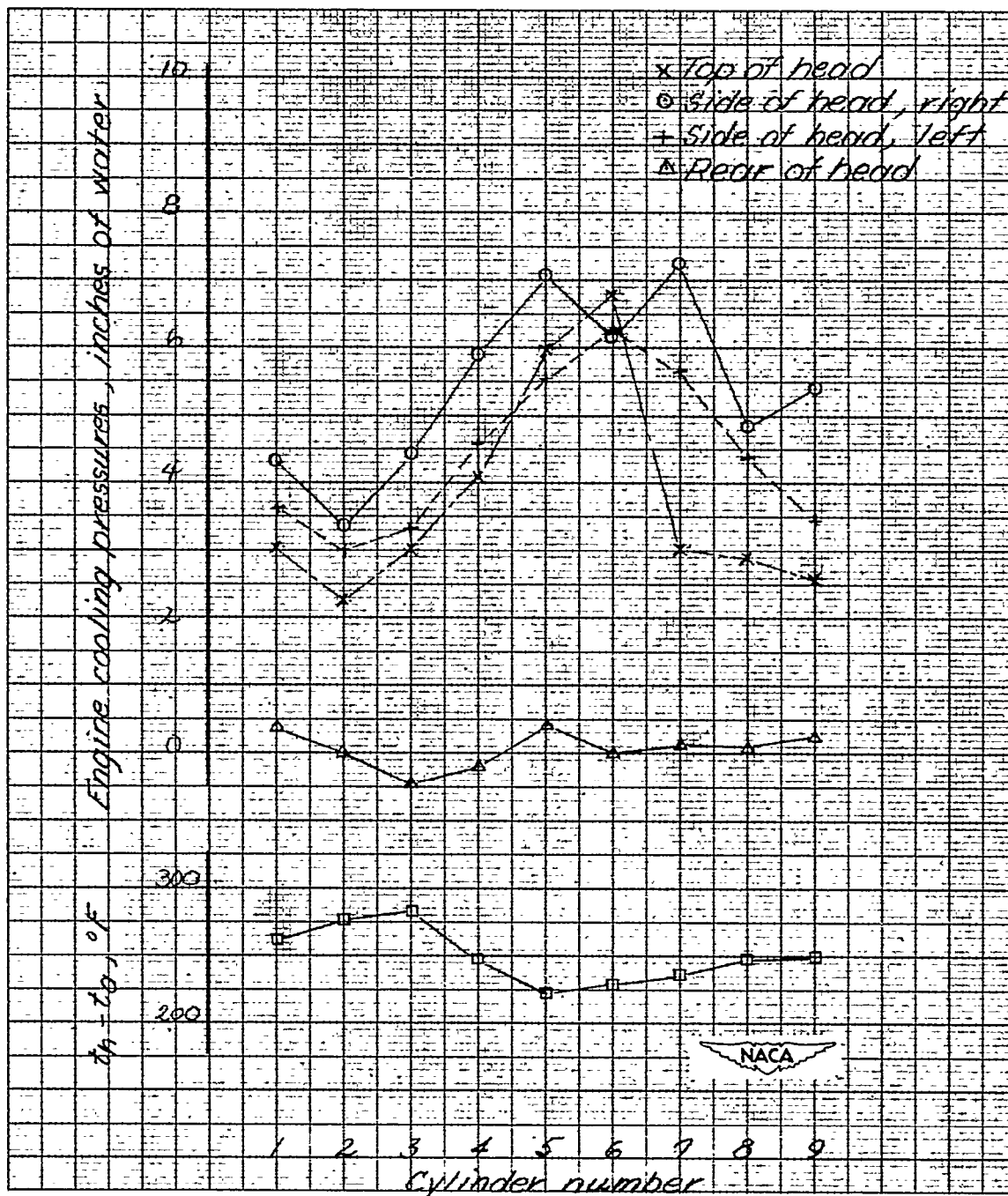
(a) 1800 rpm, 300 bhp,  $C_P = 0.08$ .

Figure 16.- Engine pressure and temperature distributions for under-slung cowling, Hamilton Standard propeller, with modified cuffs and vanes installed in cowling entrance, cowling flaps full open.



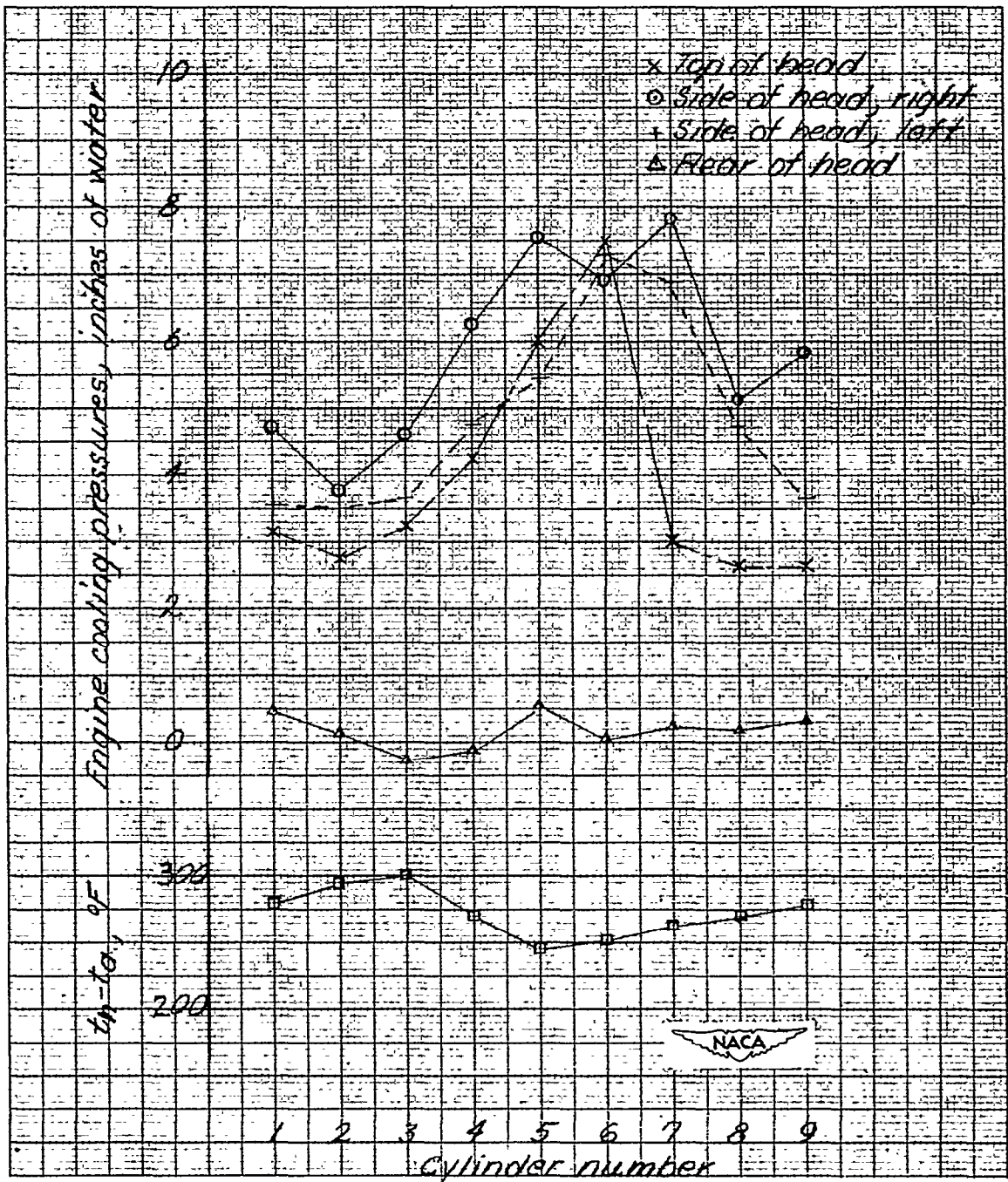
(b) 1800 rpm, 400 bhp,  $C_P = 0.11$ .

Figure 16.- Continued.



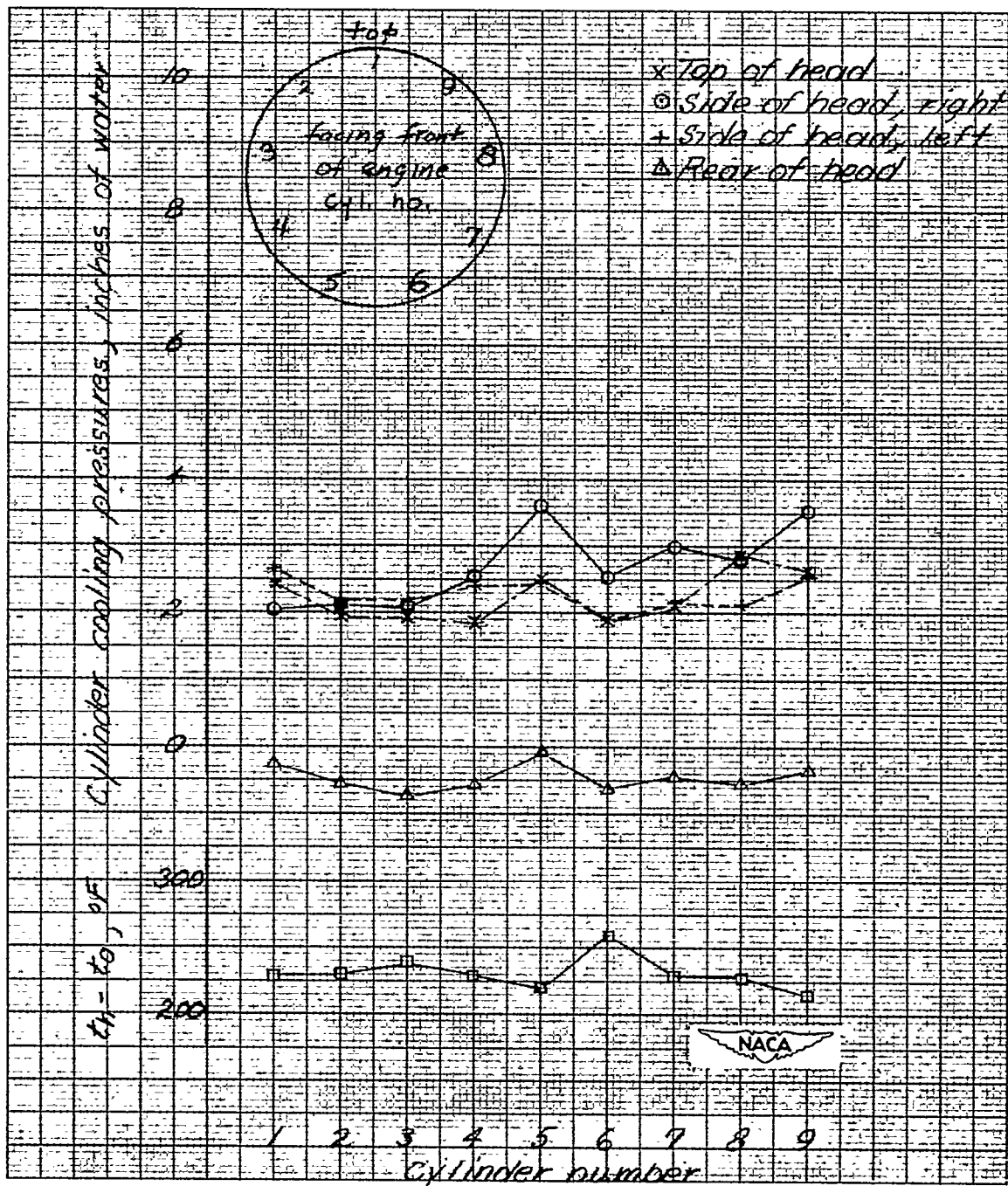
(c) 1800 rpm, 500 bhp,  $C_p = 0.13$ .

Figure 16.- Continued.



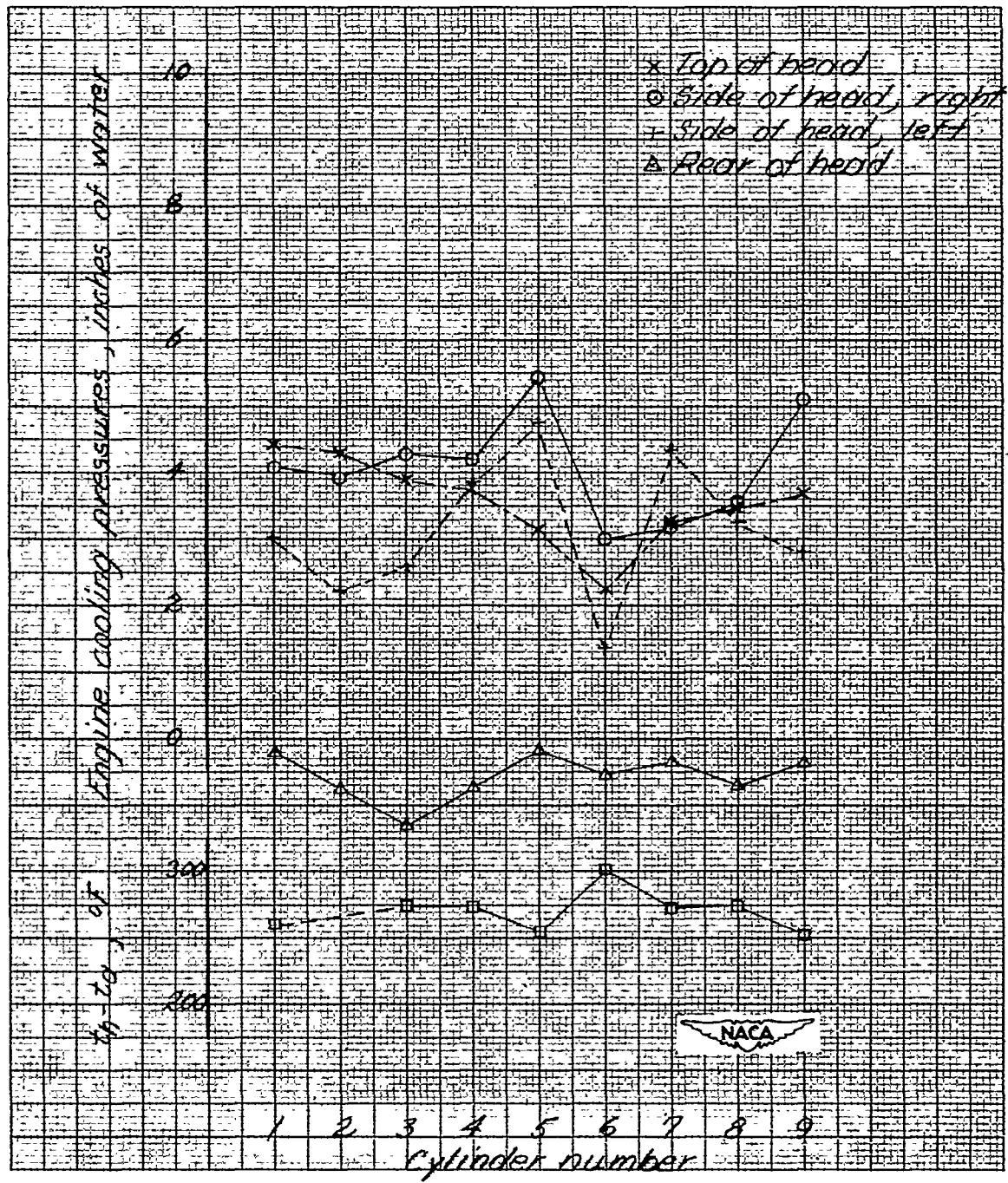
(d) 1800 rpm, 600 bhp,  $C_p = 0.16$ .

Figure 16.- Concluded.



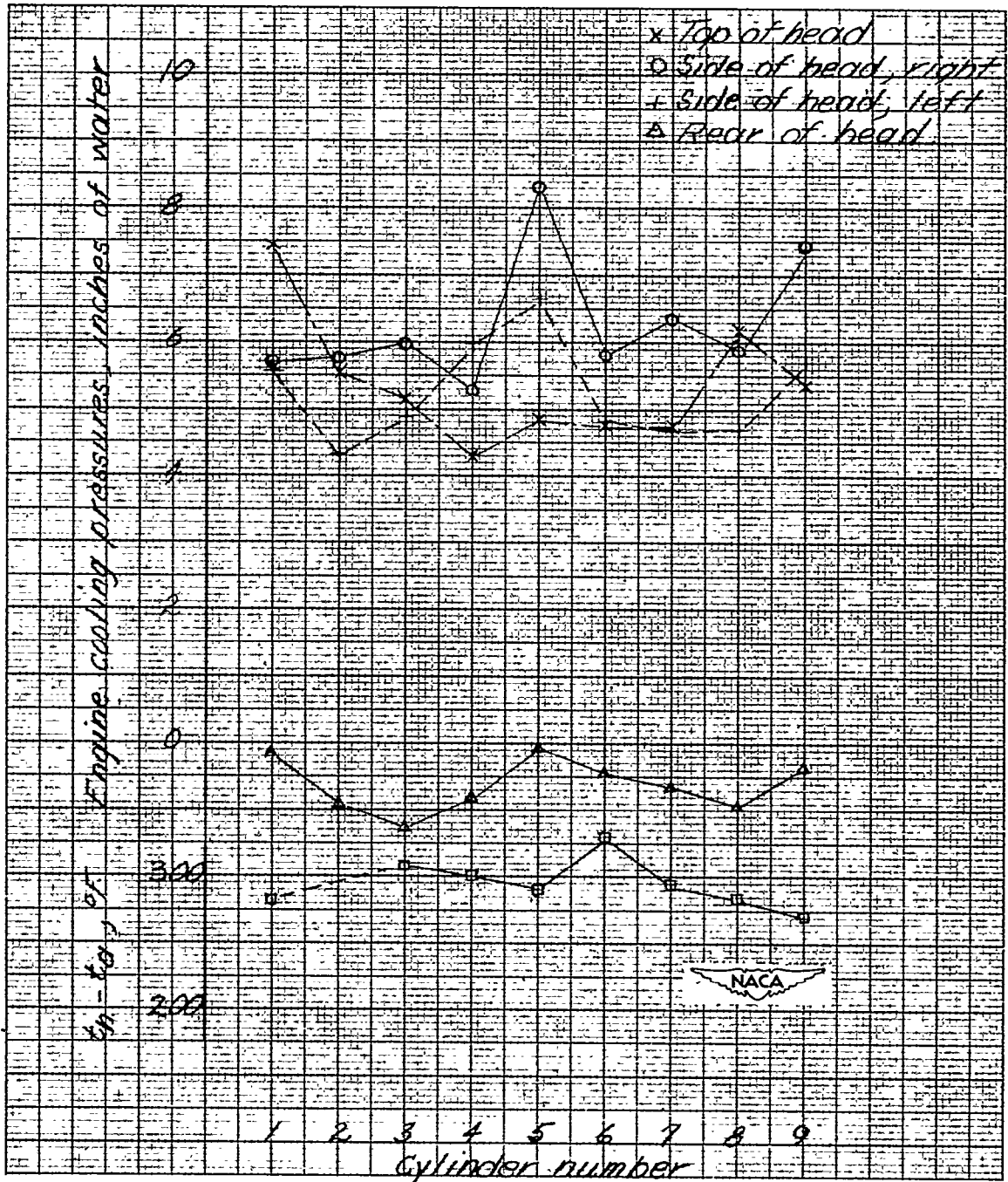
(a) 1630 rpm, 320 bhp.

Figure 17.- Engine pressure and temperature distributions for symmetrical "C" cowling, Hamilton Standard propeller with modified cuffs, cowling flaps full open.  $C_D = 0.125$ .



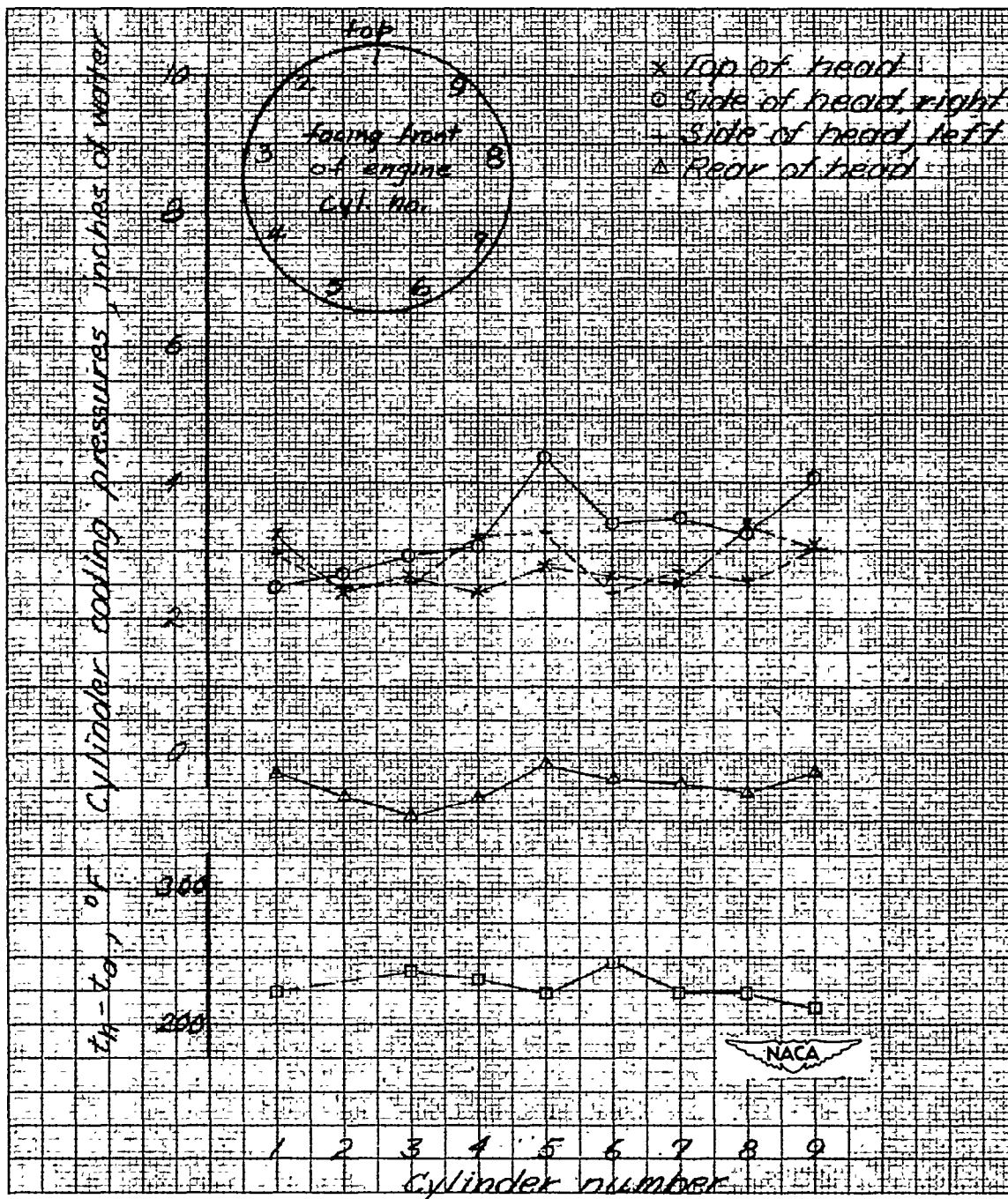
(b) 1940 rpm, 550 bhp.

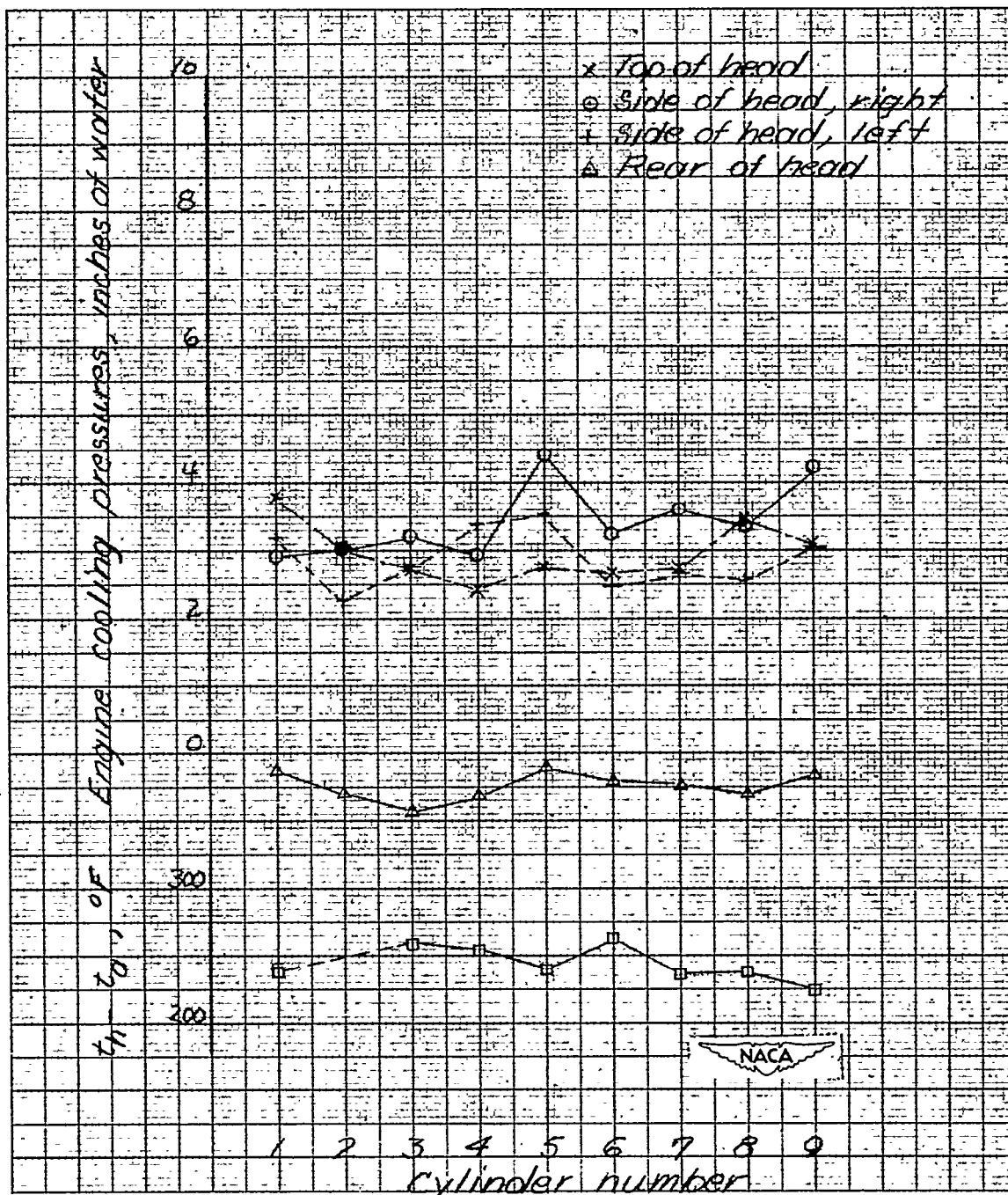
Figure 17.- Continued.



(c) 2400 rpm, 1040 bhp.

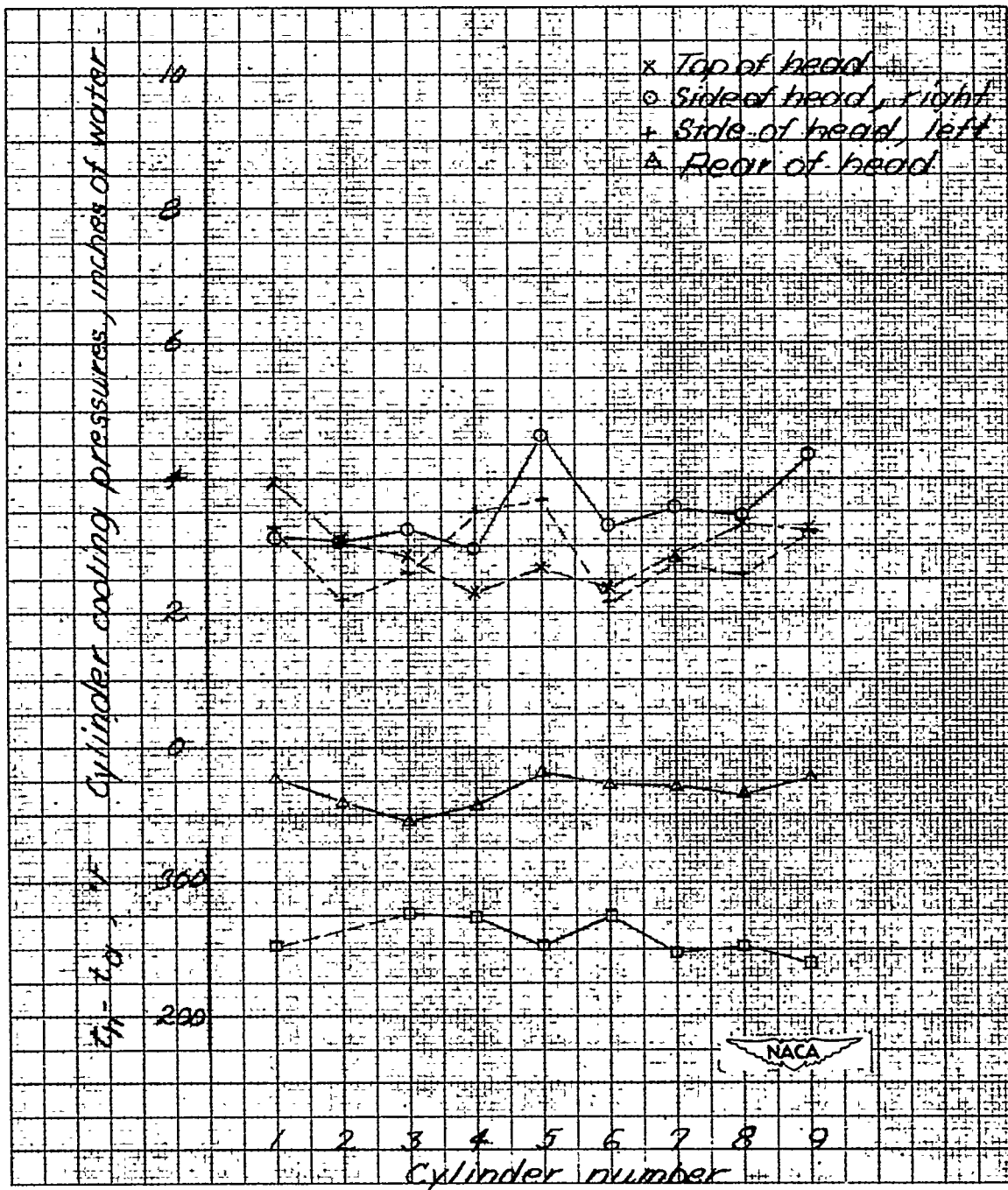
Figure 17.- Concluded.





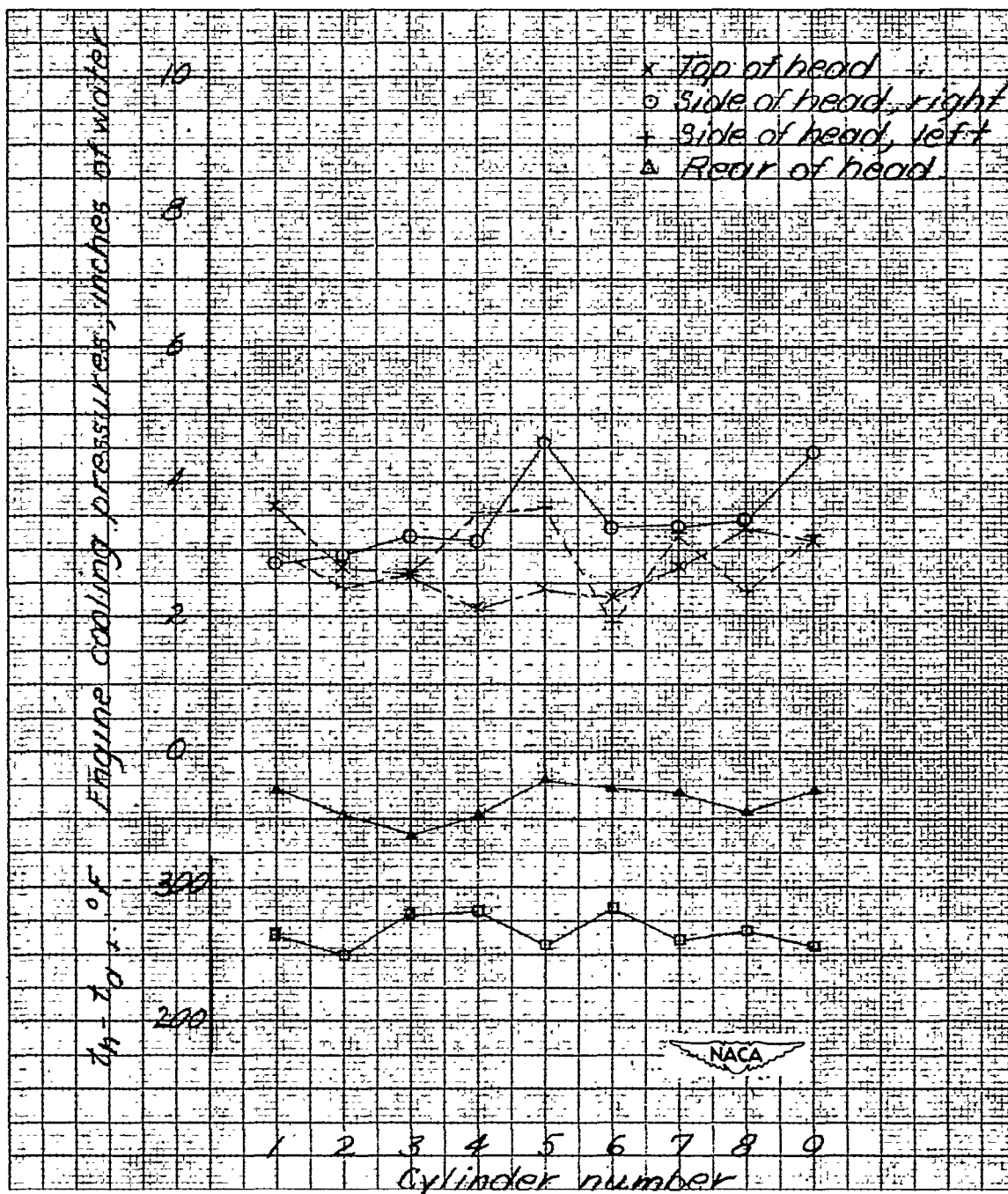
(b) 1800 rpm, 400 bhp,  $C_p = 0.11$ .

Figure 18.- Continued.



(c) 1800 rpm, 500 bhp,  $C_P = 0.13$ .

Figure 18.- Continued.



(d) 1800 rpm, 600 bhp,  $C_D = 0.16$ .

Figure 18.- Concluded.

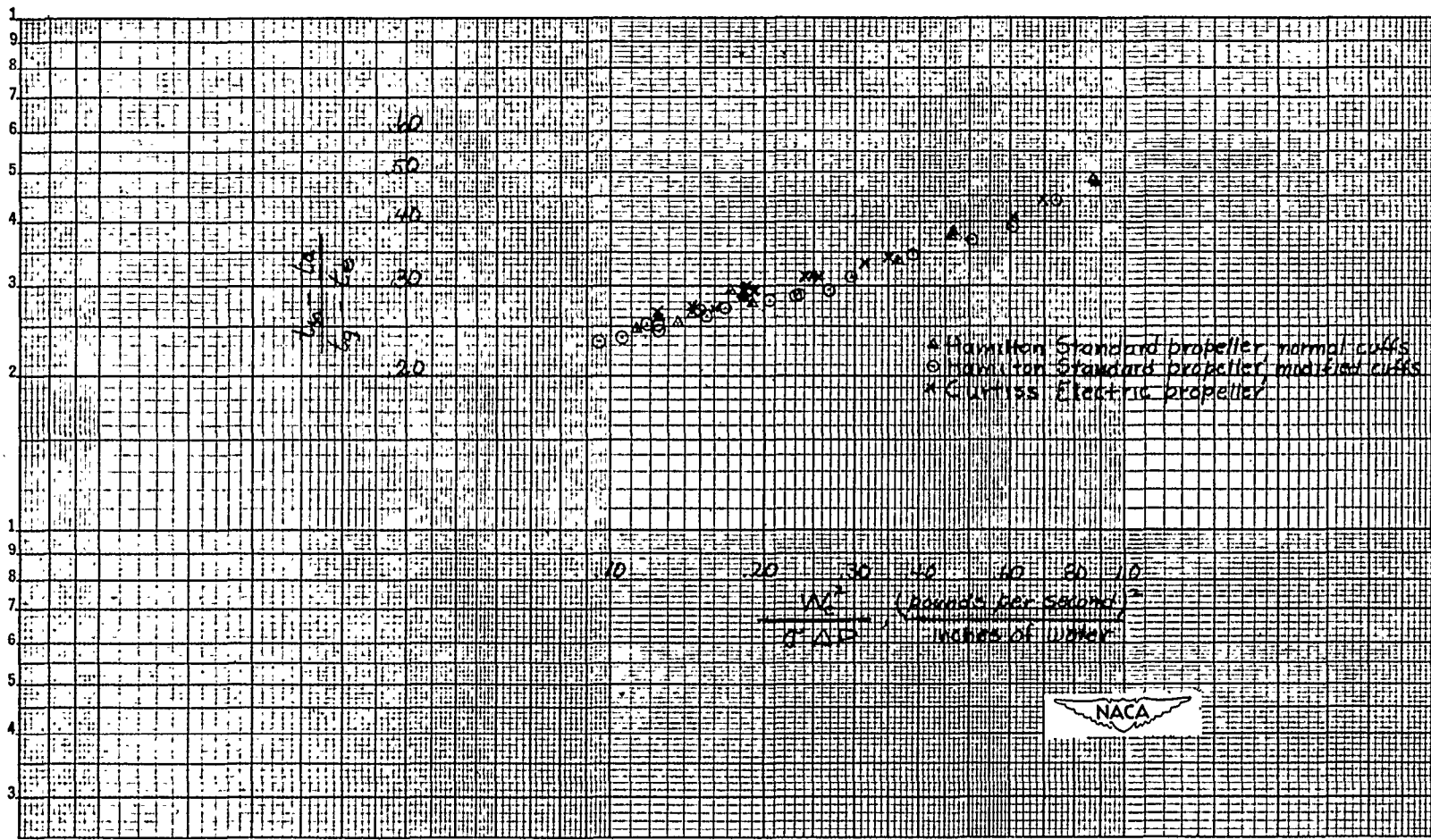
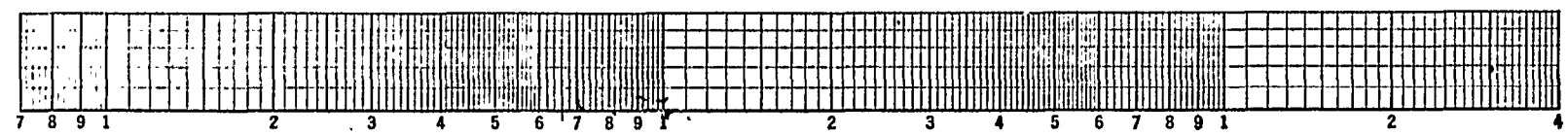


Figure 19.- Cooling correlation curves for underslung cowling with various propellers installed.



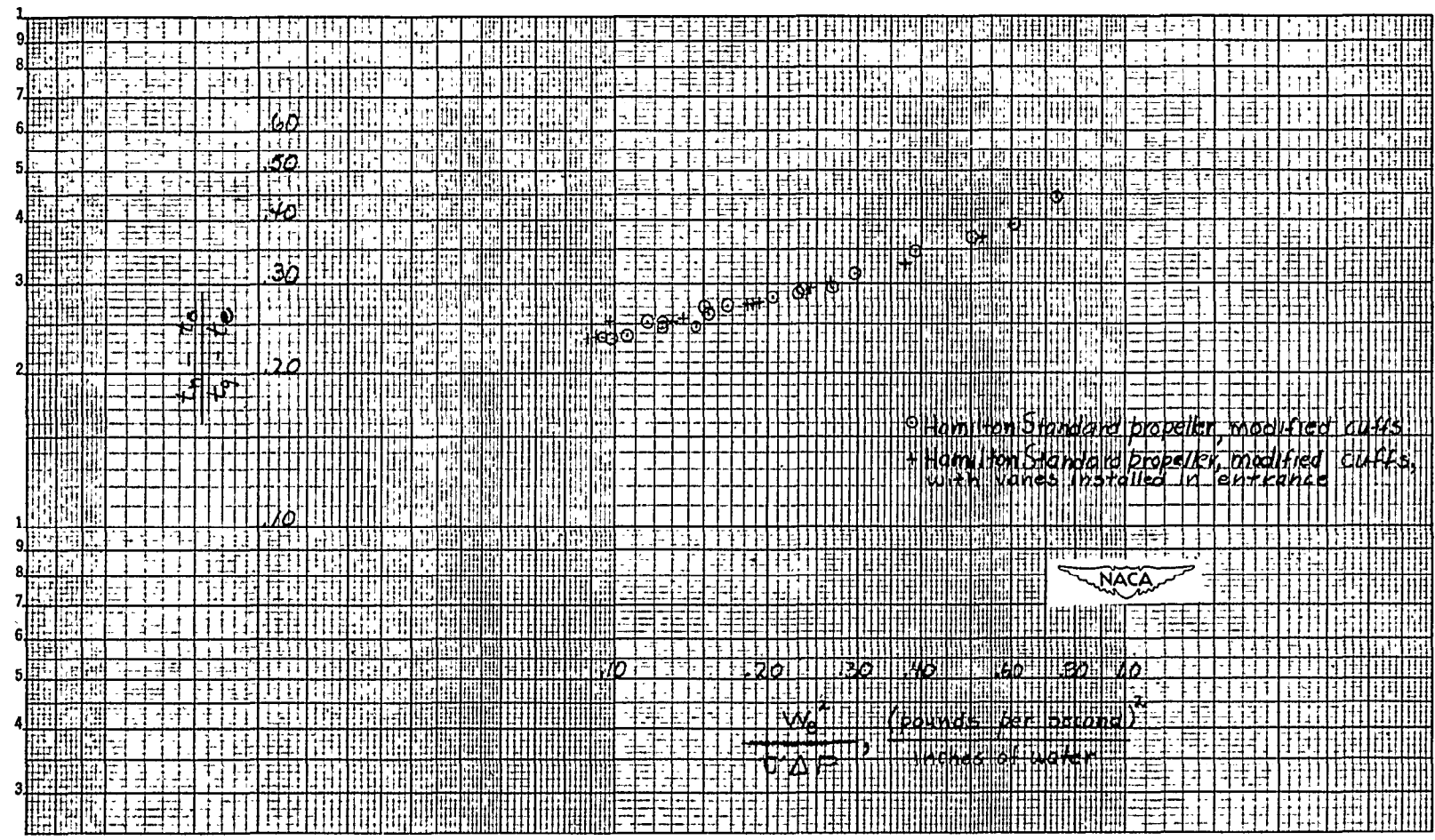


Figure 20.- Cooling correlation curves for underslung cowling with two cowling entrance configurations.

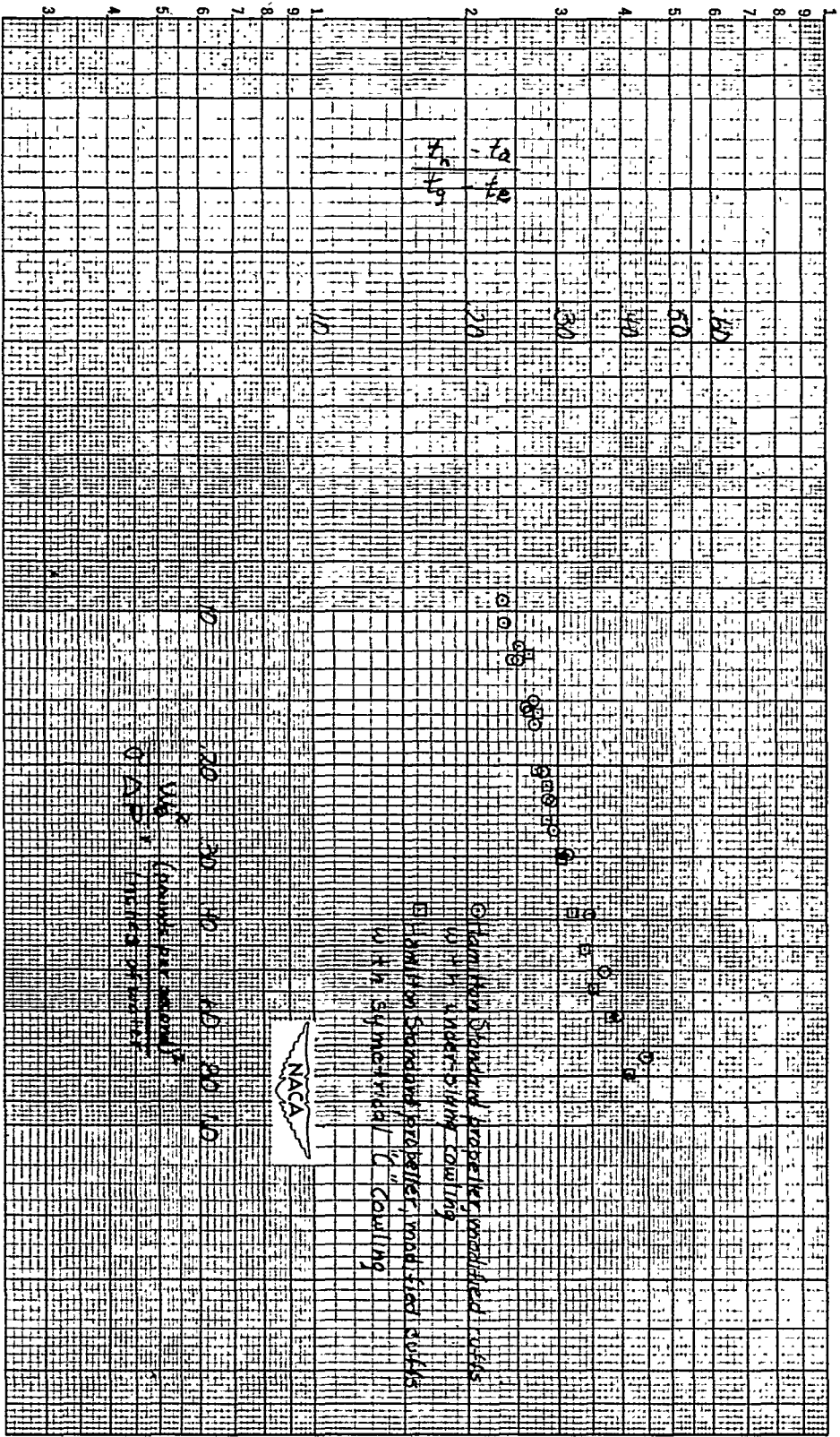


Figure 21.- Cooling correlation curves for underslung and "C" cowling with Hamilton Standard propeller with modified cuffs.

NASA Technical Library



3 1176 01437 3006